COMPARISON OF VARIOUS AUSM TYPE SCHEMES FOR THE TWO-FLUID MODEL

TORE FLÅTTEN[A] AND STEINAR EVJE[B]

ABSTRACT. In this paper we make further investigations of the *Mixture Flux* (MF) method for two-phase flows originally developed in the framework of the AUSMD scheme [12]. Here we use the method in conjunction with nonlinear state relations. We address stability and accuracy issues related to the discretization of the pressure terms, and suggest a modification that allows for a less strict stability criterion on the timestep. We further apply the framework to the two-phase AUSM$^+$ scheme of Paillère et al (2003, Comput. Fluids **32**, 891–916), denoting the resulting scheme as MF-AUSM$^+$. Comparisons between the previously developed MF-AUSMD [12] as well as the original AUSM$^+$ are made through numerical experiments. In particular, we observe that the MF-AUSM$^+$ offers significant improvements in robustness over the original AUSM$^+$.

subject classification. 76T10, 76N10, 65M12, 35L65

key words. two-phase flow, two-fluid model, hyperbolic system of conservation laws, flux splitting, explicit scheme

1. INTRODUCTION

During the last years a class of upwind schemes for the Euler equations have emerged, not being based on the characteristic field decomposition typical of approximate riemann solver schemes like the methods of Godunov and Roe. This new class of schemes, denoted as Advection Upstream Splitting Methods (AUSM) is instead based on simplified velocity and pressure splittings where the sonic waves are taken into account in the upwinding. We refer to the works of Liou et al [16, 15, 28, 7] where these methods are elaborated.

The adoptation of such schemes has been a recent and successful trend among multi-phase flow researchers. Examples include the works of Edwards et al [6] and Niu [17]. Niu explored hybrid flux-type flux splitting schemes for a multicomponent flow model, whereas Edwards et al studied a homogeneous equilibrium two-phase model with phase transitions. Characteristic for these models is that they are very similar to the Euler systems in structure and mathematical character.

Evje and Fjelde [8, 9] considered the mixture two-phase model (drift-flux model), which is a simplified isothermal two-phase model consisting of separate mass conservation equations and a mixture momentum equation. Accurate and non-oscillatory resolution of mass fronts was achieved, comparable with the Roe scheme.

In this paper we will consider a more general two-fluid model where each phase is treated separately in terms of two sets of conservation equations; one for each phase. The interaction terms between the two phases appear in the basic equations as transfer terms across the interfaces (source terms). More precisely, the basic form of the model can be written on the following vector

Date: September 25, 2003.

[A]Department of Energy and Process Engineering, Norwegian University of Science and Technology, Kolbjørn Hejes vei 1B, N-7491, Trondheim, Norway.

[B]RF-Rogaland Research, Thormøhlensgt. 55, N–5008 Bergen, Norway.

Email: tore.flatten@maskin.ntnu.no, steinar.evje@rf.no.

[B]Corresponding author.

form:

$$\partial_t \begin{pmatrix} \rho_{\rm g}\alpha_{\rm g} \\ \rho_{\rm l}\alpha_{\rm l} \\ \rho_{\rm g}\alpha_{\rm g}v_{\rm g} \\ \rho_{\rm l}\alpha_{\rm l}v_{\rm l} \end{pmatrix} + \partial_x \begin{pmatrix} \rho_{\rm g}\alpha_{\rm g}v_{\rm g} \\ \rho_{\rm l}\alpha_{\rm l}v_{\rm l} \\ \rho_{\rm g}\alpha_{\rm g}v_{\rm g}^2 + \alpha_{\rm g}p \\ \rho_{\rm l}\alpha_{\rm l}v_{\rm l}^2 + \alpha_{\rm l}p \end{pmatrix} = \begin{pmatrix} 0 \\ 0 \\ p\partial_x\alpha_{\rm g} + \tau_{\rm g} \\ p\partial_x\alpha_{\rm l} + \tau_{\rm l} \end{pmatrix} + \begin{pmatrix} 0 \\ 0 \\ Q_{\rm g} + M_{\rm g}^{\rm D} \\ Q_{\rm l} + M_{\rm l}^{\rm D} \end{pmatrix}. \tag{1}$$

Here α_k is the volume fraction of phase k with $\alpha_{\rm l} + \alpha_{\rm g} = 1$, ρ_k and v_k denote the density and fluid velocities of phase k, and p is the pressure common to both phases. Moreover, τ_k represents the interfacial forces which contain differential terms (hence, are relevant for the hyperbolicity of the model) and satisfy $\tau_{\rm g} + \tau_{\rm l} = 0$. $M_k^{\rm D}$ represents interfacial drag force with $M_{\rm g}^{\rm D} + M_{\rm l}^{\rm D} = 0$ whereas Q_k represent source terms due to gravity, friction, etc.

Paillère et al [19] investigated an extension of the AUSM$^+$ scheme of Liou [15] on the full two-fluid model, including an energy conservation equation for each phase. They found that the AUSM$^+$ scheme was able to handle a wide range of two-phase flow problems in a stable and nondissipative manner. However, the AUSM$^+$ scheme displayed a tendency towards introducing spurious oscillations and overshoots around discontinuities.

Evje and Flatten [10] investigated a related hybrid flux-splitting approach denoted as AUSMD/V on the isothermal two-fluid model. The advantage of this approach is that robust resolution of sonic waves may be achieved without the inclusion of additional low Mach number pressure diffusion terms [7, 8, 19].

However, the AUSMD/V approach suffers from the same problems as AUSM$^+$ regarding accurate and robust resolution of discontinuities associated with the volume fraction waves. As far as the current two-fluid model is concerned, the wave phenomena depend strongly on properties of the mixture and involve expressions where the phasic variables are tightly coupled [5, 10]. The AUSM class of schemes solves each phasic set of equations independently and these couplings are not fully taken into account.

The AUSMD scheme was later refined [12] by enforcing a stronger coupling between the phasic variables in the numerical resolution algorithm, leading to the concept of *Mixture Flux* (MF) methods. Using this approach numerical oscillations were removed, and the resulting MF-AUSMD scheme was demonstrated to possess accuracy and robustness properties on level with the Roe scheme.

The starting point of the present work is two basic AUSM$^+$ type schemes similar to those studied by Paillère et al [19]. A main objective of this work is to understand more precisely where the MF class of schemes stand when they are compared to these two basic AUSM$^+$ schemes.

The MF methods are first presented in a semidiscrete setting, similar to the one introduced in [11]. Particularly, the MF methods are constructed so that they satisfy the following "good" properties: (i) The numerical mass fluxes reduce to upwind type of fluxes for a linear contact discontinuity similar to those produced by an exact Riemann solver; (ii) Abgrall's principle is satisfied; that is, a flow uniform in velocity and pressure, must remain uniform during its temporal evolution.

A special feature of the MF approach is that one systematically makes use of the following pressure evolution equation

$$\frac{\partial p}{\partial t} + \kappa \left(\rho_{\rm l} \frac{\partial}{\partial x} \left(\rho_{\rm g}\alpha_{\rm g}v_{\rm g} \right) + \rho_{\rm g} \frac{\partial}{\partial x} \left(\rho_{\rm l}\alpha_{\rm l}v_{\rm l} \right) \right) = 0, \tag{2}$$

where

$$\kappa = \frac{1}{\frac{\partial \rho_{\rm l}}{\partial p}\alpha_{\rm l}\rho_{\rm g} + \frac{\partial \rho_{\rm g}}{\partial p}\alpha_{\rm g}\rho_{\rm l}}, \tag{3}$$

for the construction of a suitable numerical flux associated with the pressure.

The original MF approach, as described in [12], employed a straightforward Lax-Friedrichs-like discretization of the pressure evolution equation (2). In [12] the resulting MF-AUSMD scheme was compared with a Roe scheme and we observed that the resolution of the sonic waves was slightly more diffusive for the MF-AUSMD scheme. One of the purposes of this work is to eliminate this drawback. More precisely, the main contributions of this work can be summarized as follows:

(1) We provide more insight into mechanisms which are important for accurate and robust resolution of the various waves by comparing two basic AUSM$^+$ schemes, similar to those studied by Paillère et al [19], to corresponding Mixture Flux (MF) type AUSM schemes derived within the framework of [12].
(2) We demonstrate that the MF approach does not depend strongly on the particular form of the basis flux used for the discretization of the convective fluxes. Particularly, we construct an AUSM$^+$ based mixture flux scheme, denoted as MF-AUSM$^+$. We perform numerical experiments indicating that the mixture flux method acts upon AUSM$^+$ by reducing numerical oscillations while maintaining the desirable nondissipative properties around discontinuities. Hence the picture observed for the MF-AUSMD [12] is maintained, demonstrating the general applicability of the MF class of schemes.
(3) We show that the MF approach presented in [12] leads to a stability criterion for the timestep which is more strict than the standard CFL criterion

$$\frac{\Delta x}{\Delta t} \geq \lambda_{\max}, \tag{4}$$

where $\lambda_{\max}$ is the fastest characteristic velocity for the system.

By way of an argument based on simplified assumptions, a modification of the MF approach is suggested where we rescale the numerical diffusion coefficients to act more as an "upwind" type of numerical viscosity. We demonstrate that this "upwind" rescaling fixes the above problem, i.e. the resulting MF-schemes are stable under the CFL condition (4). Within this framework, denoted as *Rescaled Mixture Flux* (RMF), the poorer stability properties of AUSM$^+$ on sonic waves resurface. We observe that the accuracy in the resolution of sonic waves for RMF-AUSMD is very similar to a Roe scheme whereas RMF-AUSM$^+$ tends to produce small overshoots, demonstrating that the AUSMD seems to be the most promising candidate for the convective flux splitting.

The paper is organized as follows: In Section 2 we state the two-fluid model we will be working with. In Section 3 we restate two basic AUSM$^+$ schemes for the isothermal two-fluid model similar to those presented in [19] for the full non-isothermal two-fluid model. In Section 4 we give a general presentation of the class of Mixture Flux (MF) schemes in a semi-discrete setting. In Section 5 we construct three fully discrete MF schemes denoted as MF-AUSMD, MF-AUSM$^+$, and MF-CVS. The only difference between these schemes lies in the choice of the numerical convective fluxes associated with the $\alpha\rho v$ and $\alpha\rho v^2$ terms. In Section 6 we introduce a *viscosity rescaling* refinement to the MF framework, improving the accuracy and efficiency on sonic waves. In particular, this brings forth rescaled versions of the MF schemes, denoted as RMF type schemes. In Section 7 we perform numerical simulations comparing the performance of the various schemes. Finally the basic results and conclusions of the paper are summarized.

2. The Two-Fluid Model

Throughout this paper we will be concerned with the common two-fluid model formulated by stating separate conservation equations for mass and momentum for the two fluids, which we will denote as a gas (g) and a liquid (l) phase. The model is identical to the model previously considered by Paillère et al [19] and will be briefly stated here. We let $\mathbf{U}$ be the vector of conserved variables

$$\mathbf{U} = \begin{bmatrix} \rho_{\mathrm{g}}\alpha_{\mathrm{g}} \\ \rho_{\mathrm{l}}\alpha_{\mathrm{l}} \\ \rho_{\mathrm{g}}\alpha_{\mathrm{g}}v_{\mathrm{g}} \\ \rho_{\mathrm{l}}\alpha_{\mathrm{l}}v_{\mathrm{l}} \end{bmatrix} = \begin{bmatrix} m_{\mathrm{g}} \\ m_{\mathrm{l}} \\ I_{\mathrm{g}} \\ I_{\mathrm{l}} \end{bmatrix}. \tag{5}$$

By using the notation $\Delta p = p - p^i$, where p^i is the interfacial pressure, and $\tau_k = (p^i - p)\partial_x \alpha_k$, we see that the model (1) can be written on the form

- Conservation of mass

$$\frac{\partial}{\partial t}\left(\rho_{\mathrm{g}}\alpha_{\mathrm{g}}\right) + \frac{\partial}{\partial x}\left(\rho_{\mathrm{g}}\alpha_{\mathrm{g}}v_{\mathrm{g}}\right) = 0, \tag{6}$$

$$\frac{\partial}{\partial t}\left(\rho_{\mathrm{l}}\alpha_{\mathrm{l}}\right)+\frac{\partial}{\partial x}\left(\rho_{\mathrm{l}}\alpha_{\mathrm{l}}v_{\mathrm{l}}\right)=0, \tag{7}$$

- Conservation of momentum

$$\frac{\partial}{\partial t}\left(\rho_{\mathrm{g}}\alpha_{\mathrm{g}}v_{\mathrm{g}}\right)+\frac{\partial}{\partial x}\left(\rho_{\mathrm{g}}\alpha_{\mathrm{g}}v_{\mathrm{g}}^2+\alpha_{\mathrm{g}}p\right)+(\Delta p-p)\frac{\partial\alpha_{\mathrm{g}}}{\partial x}=Q_{\mathrm{g}}+M_{\mathrm{g}}^{\mathrm{D}}, \tag{8}$$

$$\frac{\partial}{\partial t}\left(\rho_{\mathrm{l}}\alpha_{\mathrm{l}}v_{\mathrm{l}}\right)+\frac{\partial}{\partial x}\left(\rho_{\mathrm{l}}\alpha_{\mathrm{l}}v_{\mathrm{l}}^2+\alpha_{\mathrm{l}}p\right)+(\Delta p-p)\frac{\partial\alpha_{\mathrm{l}}}{\partial x}=Q_{\mathrm{l}}+M_{\mathrm{l}}^{\mathrm{D}}, \tag{9}$$

Alternatively, the momentum conservation equations may be written on the equivalent form

$$\frac{\partial}{\partial t}\left(\rho_{\mathrm{g}}\alpha_{\mathrm{g}}v_{\mathrm{g}}\right)+\frac{\partial}{\partial x}\left(\rho_{\mathrm{g}}\alpha_{\mathrm{g}}v_{\mathrm{g}}^2\right)+\alpha_{\mathrm{g}}\frac{\partial p}{\partial x}+(\Delta p)\frac{\partial\alpha_{\mathrm{g}}}{\partial x}=Q_{\mathrm{g}}+M_{\mathrm{g}}^{\mathrm{D}}, \tag{10}$$

$$\frac{\partial}{\partial t}\left(\rho_{\mathrm{l}}\alpha_{\mathrm{l}}v_{\mathrm{l}}\right)+\frac{\partial}{\partial x}\left(\rho_{\mathrm{l}}\alpha_{\mathrm{l}}v_{\mathrm{l}}^2\right)+\alpha_{\mathrm{l}}\frac{\partial p}{\partial x}+(\Delta p)\frac{\partial\alpha_{\mathrm{l}}}{\partial x}=Q_{\mathrm{l}}+M_{\mathrm{l}}^{\mathrm{D}}. \tag{11}$$

2.1. **Submodels.** For the numerical simulations presented in this work we follow Paillère et al [19] and use thermodynamic relations representative of water and air, derived under the assumption of constant entropies.

For the gas phase we have

$$\rho_{\mathrm{g}}(p)=\widehat{\rho_{\mathrm{g}}}\left(\frac{p}{C}\right)^{1/\gamma}, \tag{12}$$

where $C=10^5$ Pa, $\widehat{\rho_{\mathrm{g}}}=1$ kg/m^3 and $\gamma=1.4$. The sound velocity is given by

$$a_{\mathrm{g}}^2=\frac{\partial p}{\partial\rho_{\mathrm{g}}}=\frac{\gamma p}{\rho_{\mathrm{g}}}. \tag{13}$$

For the liquid phase we have

$$\rho_{\mathrm{l}}=\widehat{\rho_{\mathrm{l}}}\left(\frac{p}{B}+1\right)^{1/n}, \tag{14}$$

where $\widehat{\rho_{\mathrm{l}}}=10^3$ kg/m^3, $B=3.3\cdot10^5$ Pa and $n=7.15$. The sound velocity is given by

$$a_{\mathrm{l}}^2=\frac{\partial p}{\partial\rho_{\mathrm{l}}}=\frac{n}{\rho_{\mathrm{l}}}\left(p+B\right). \tag{15}$$

Moreover, we will treat Q_k as a pure source term, assuming that it does not contain any differential operators. We use the interface pressure correction

$$\Delta p=\sigma\frac{\alpha_{\mathrm{g}}\alpha_{\mathrm{l}}\rho_{\mathrm{g}}\rho_{\mathrm{l}}}{\rho_{\mathrm{g}}\alpha_{\mathrm{l}}+\rho_{\mathrm{l}}\alpha_{\mathrm{g}}}(v_{\mathrm{g}}-v_{\mathrm{l}})^2, \tag{16}$$

where throughout this paper we use $\sigma=1.2$, ensuring a hyperbolic model.

Having solved for the conservative variables $\mathbf{U}$, we need to obtain the primitive variables $(\alpha_{\mathrm{g}},p,v_{\mathrm{g}},v_{\mathrm{l}})$. For the pressure variable we see that by writing the volume fraction equation $\alpha_{\mathrm{g}}+\alpha_{\mathrm{l}}=1$ in terms of the conserved variables as

$$\frac{m_{\mathrm{g}}}{\rho_{\mathrm{g}}(p)}+\frac{m_{\mathrm{l}}}{\rho_{\mathrm{l}}(p)}=1, \tag{17}$$

we obtain a relation yielding the pressure $p(m_{\mathrm{g}},m_{\mathrm{l}})$. This is a nonlinear equation which does not easily allow for an algebraic solution. Instead we use an iterative numerical algorithm to obtain the pressure from (17).

Moreover, the fluid velocities v_{g} and v_{l} are obtained directly from the relations

$$v_{\mathrm{g}}=\frac{U_3}{U_1},\qquad v_{\mathrm{l}}=\frac{U_4}{U_2}.$$

Paillère et al [19] considered a more general model where conservation of total energy for each phase was included. Throughout this work we will study only the isentropic 4-equation model given above. The inclusion of energy equations does not significantly alter the existing eigenstructure of the isentropic model, but adds entropy waves moving with the fluid velocities. It is therefore our belief that the main difficulties related to the strong phasic couplings in the pressure and volume fraction waves are fully present in the isentropic model.

2.2. **Wave Phenomena.** The phasic sonic velocities are given by $a_{\rm g}$ (13) and $a_{\rm l}$ (15), satisfying

$$a_k^2 \equiv \frac{\partial p}{\partial \rho_k}. \tag{18}$$

However, we note that the model possesses two characteristic sonic wave velocities approximately given by

$$\lambda^{\rm p} = \bar{v}^{\rm p} \pm c, \tag{19}$$

where

$$\bar{v}^{\rm p} = \frac{\rho_{\rm g}\alpha_{\rm l} v_{\rm l} + \rho_{\rm l}\alpha_{\rm g} v_{\rm g}}{\rho_{\rm g}\alpha_{\rm l} + \rho_{\rm l}\alpha_{\rm g}} \tag{20}$$

and c is a mathematical *mixture* sound velocity approximately given by

$$c = \sqrt{\frac{\rho_{\rm l}\alpha_{\rm g} + \rho_{\rm g}\alpha_{\rm l}}{\frac{\partial \rho_{\rm g}}{\partial p}\rho_{\rm l}\alpha_{\rm g} + \frac{\partial \rho_{\rm l}}{\partial p}\rho_{\rm g}\alpha_{\rm l}}}. \tag{21}$$

In addition, the model possesses two characteristic volume fraction wave velocities approximately given by

$$\lambda^{\alpha} = \bar{v}^{\alpha} \pm \gamma, \tag{22}$$

where

$$\bar{v}^{\alpha} = \frac{\rho_{\rm g}\alpha_{\rm l} v_{\rm g} + \rho_{\rm l}\alpha_{\rm g} v_{\rm l}}{\rho_{\rm g}\alpha_{\rm l} + \rho_{\rm l}\alpha_{\rm g}} \tag{23}$$

and

$$\gamma = \sqrt{\frac{\Delta p(\rho_{\rm g}\alpha_{\rm l} + \rho_{\rm l}\alpha_{\rm g}) - \rho_{\rm l}\rho_{\rm g}\alpha_{\rm l}\alpha_{\rm g}(v_{\rm g} - v_{\rm l})^2}{(\rho_{\rm g}\alpha_{\rm l} + \rho_{\rm l}\alpha_{\rm g})^2}}. \tag{24}$$

These approximations are derived under the assumption that $|v_{\rm g} - v_{\rm l}| << c$. We refer to [26, 10] for more details.

Remark 1. *Using an interface pressure correction term of the form* (16)*, we see that the approximate volume fraction velocity* (24) *becomes imaginary if* $\sigma \leq 1$*. Choosing* $\sigma \geq 1$ *we obtain real-valued wave velocities and a hyperbolic model.*

3. Two AUSM$^+$ Schemes

We now consider the basic system (6)–(9), and assume it is discretized on the following form:

$$\begin{aligned} \mathbf{U}_j^{n+1} = \mathbf{U}_j^n &- \frac{\Delta t}{\Delta x}\left(\mathbf{F}^c(\mathbf{U}_j^n, \mathbf{U}_{j+1}^n) - \mathbf{F}^c(\mathbf{U}_{j-1}^n, \mathbf{U}_j^n)\right) \\ &- \frac{\Delta t}{\Delta x}\left(\mathbf{F}^p(\mathbf{U}_j^n, \mathbf{U}_{j+1}^n) - \mathbf{F}^p(\mathbf{U}_{j-1}^n, \mathbf{U}_j^n)\right) \\ &- \Delta t\left([\Delta p - p]\partial_x \mathbf{H}\right)_j^n + \Delta t \mathbf{Q}_j^n. \end{aligned} \tag{25}$$

Here $\mathbf{F}^c$ and $\mathbf{F}^p$ are numerical fluxes assumed to be consistent with the corresponding physical fluxes $\mathbf{f}^c$ and $\mathbf{f}^p$,

$$\mathbf{f}^c = \begin{pmatrix} \rho_{\rm g}\alpha_{\rm g} v_{\rm g} \\ \rho_{\rm l}\alpha_{\rm l} v_{\rm l} \\ \rho_{\rm g}\alpha_{\rm g} v_{\rm g}^2 \\ \rho_{\rm l}\alpha_{\rm l} v_{\rm l}^2 \end{pmatrix}, \qquad \mathbf{f}^p = \begin{pmatrix} 0 \\ 0 \\ \alpha_{\rm g} p \\ \alpha_{\rm l} p \end{pmatrix},$$

and $\mathbf{H}$ and $\mathbf{Q}$ is given by

$$\mathbf{H} = \begin{pmatrix} 0 \\ 0 \\ \alpha_{\rm g} \\ \alpha_{\rm l} \end{pmatrix}, \qquad \mathbf{Q} = \begin{pmatrix} 0 \\ 0 \\ Q_{\rm g} \\ Q_{\rm l} \end{pmatrix}.$$

We see that the fluxes of the the model (6)–(9) consist of three different sort of terms; convective flux terms $\partial_x(\rho\alpha v)$ and $\partial_x(\rho\alpha v^2)$, conservative pressure terms $\partial_x(\alpha p)$ and non-conservative pressure terms $[\Delta p - p]\partial_x \alpha$. The discretization of these terms as described below closely follows the work of Paillère et al [19].

3.1. **Convective fluxes.** For phase k we assume a numerical velocity of sound $c_k = [c_k]_{j+1/2}$ at the cell interface, to be defined below. Following Liou [15] and in turn Paillère et al [19], we further consider the velocity splitting formulas

$$V^{\pm}(v,c) = \begin{cases} \pm\frac{1}{4c}(v \pm c)^2 \pm \frac{1}{8c^3}(v^2 - c^2)^2 & \text{if } |v| \le c \\ \frac{1}{2}(v \pm |v|) & \text{otherwise.} \end{cases} \tag{26}$$

For each phase we now define the cell interface velocity $v_{j+1/2}$ as

$$v_{j+1/2} = V^{+}(v_j, c_{j+1/2}) + V^{-}(v_{j+1}, c_{j+1/2}), \tag{27}$$

obtaining the convective mass flux

$$(\rho\alpha v)_{j+1/2} = \begin{cases} (\rho\alpha)_j v_{j+1/2} & \text{if } v_{j+1/2} \ge 0 \\ (\rho\alpha)_{j+1} v_{j+1/2} & \text{otherwise.} \end{cases} \tag{28}$$

From this we construct the convective momentum flux

$$(\rho\alpha v^2)_{j+1/2} = \begin{cases} (\rho\alpha v)_{j+1/2} v_j & \text{if } (\rho\alpha v)_{j+1/2} \ge 0 \\ (\rho\alpha v)_{j+1/2} v_{j+1} & \text{otherwise.} \end{cases} \tag{29}$$

3.2. **Pressure fluxes.** We discretize the conservative pressure term as

$$(\alpha p)_{j+1/2} = P^{+}(v_j, c_{j+1/2})(\alpha p)_j + P^{-}(v_{j+1}, c_{j+1/2})(\alpha p)_{j+1} \tag{30}$$

where the pressure splitting formulas are given as

$$P^{\pm} = \begin{cases} \frac{1}{4c}(v \pm c)^2(2 \mp \frac{v}{c}) \pm \frac{3}{16c^5} v(v^2 - c^2)^2 & \text{if } |v| \le c \\ \frac{1}{2}(1 \pm \mathrm{sgn}(v)) & \text{otherwise.} \end{cases} \tag{31}$$

3.3. **Definition of cell interface sound velocity.** To define the sound velocities at the cell interface we use the expression

$$[c_k]_{j+1/2} = \sqrt{[c_k]_j [c_k]_{j+1}} \tag{32}$$

for both phases. Here $c_{\mathrm{g}} = a_{\mathrm{g}}$ and $c_{\mathrm{l}} = a_{\mathrm{l}}$ given by (13) and (15), in accordance with Paillére et al [19].

Remark 2. *Another natural choice, more in accordance with the mixture nature of the model, is to use the mixture sound velocity* c_{mix} *given by* (21). *That is, for the splitting formulas* (26) *we could use*

$$c_{\mathrm{g}} = c_{\mathrm{l}} = c_{\mathrm{mix}}. \tag{33}$$

Such a choice was considered in [8] *for the mixture model and in* [10] *for the two-fluid model. For two-phase flows, the numerical performance of the AUSM scheme may not be strongly dependent on the choice of expression for the numerical sound velocity* [9].

3.4. **Low Mach number flows.** Paillére et al [19] noted the need to couple the pressure and velocity fields for low speeds, as the AUSM$^+$ scheme acts much like a central difference scheme in the low Mach number limit. This may lead to oscillations due to odd-even decoupling. The problem is particularly relevant for the near incompressible (i.e. liquid) phase, as the sound velocity may here become very large. To remedy the situation, Paillére et al suggested following the approach of Edwards [7], modifying the liquid mass flux as described by the steps below.

(1) Calculate the basic AUSM$^+$ mass flux $(\rho_{\mathrm{l}}\alpha_{\mathrm{l}}v_{\mathrm{l}})_{j+1/2}$ as given by (28).

(2) Define a cell interface Mach number $M_{j+1/2}$ as follows:

$$M_{j+1/2} = \frac{1}{2}\left(\left(\frac{v_{\mathrm{l}}}{c_{\mathrm{l}}}\right)_j + \left(\frac{v_{\mathrm{l}}}{c_{\mathrm{l}}}\right)_{j+1}\right). \tag{34}$$

(3) Define a *scaling factor* $f(M)$ as

$$f(M) = \frac{\sqrt{\left(1 - M_0^2\right)^2 M^2 + 4M_0^2}}{1 + M_0^2}, \tag{35}$$

where the parameter M_0 is a "cut-off" Mach number.

(4) Rescale the cell interface sound velocity $c_{j+1/2}$ as follows

$$\widehat{c_l} = f(M_{j+1/2})[c_l]_{j+1/2}. \tag{36}$$

(5) Compute a rescaled interface liquid velocity correction as

$$\widehat{[v_l]}_{j+1/2} = V^+([v_l]_j, \widehat{c_l}) - \frac{1}{2}([v_l]_j + |[v_l]_j|) - V^-([v_l]_{j+1}, \widehat{c_l}) - \frac{1}{2}([v_l]_{j+1} + |[v_l]_{j+1}|), \tag{37}$$

where the splitting formulas $V^\pm$ are the AUSM$^+$ splitting formulas (26).

(6) Evaluate the pressure diffusion term as

$$D_{j+1/2} = \frac{1}{2}\left(\frac{1}{M_0^2} - 1\right)\widehat{[v_l]}_{j+1/2}\frac{(\alpha_l p)_j - (\alpha_l p)_{j+1}}{[c_l]^2_{j+1/2}}. \tag{38}$$

(7) Modify the liquid mass flux

$$\widehat{(\rho_l \alpha_l v_l)}_{j+1/2} = (\rho_l \alpha_l v_l)_{j+1/2} + D_{j+1/2}. \tag{39}$$

The diffusion term $D_{j+1/2}$ has a stabilizing effect on oscillations in the pressure variable, and vanishes for smooth flows. The disadvantage of this approach is that the parameter M_0 may require some tuning.

3.5. **Non-Conservative Differential Terms.** For the spatial term on the form $p\partial_x\alpha$ we follow the approach of Coquel et al [4] and Paillère et al [19] who suggested a central differencing. That is, we write

$$\left([\Delta p - p]\frac{\partial \alpha}{\partial x}\right)_j = [\Delta p - p]_j \frac{\alpha_{j+1} - \alpha_{j-1}}{2\Delta x}. \tag{40}$$

3.6. **Two AUSM type schemes.** Based on the above specifications we introduce the two following definitions:

Definition 1. *We will use the term* **AUSM$^+$** *to denote the numerical algorithm obtained from* (25) *by using the convective fluxes* (28) *and* (29)*, the conservative pressure flux* (30)*, and the non-conservative pressure flux* (40)*.*

Definition 2. *We will use the term* **PD-AUSM$^+$** *to denote the numerical algorithm obtained as for the AUSM$^+$ scheme but where pressure diffusion has been introduced for the liquid mass flux as described by* (34)–(39)*.*

4. The MF (Mixture Flux) Class of schemes

4.1. **General form.** In this section we first present the MF class of schemes in a semi-discrete setting. Fully discrete approximations of the model (6)–(9) are then obtained in Section 5. The starting point is the model (6)–(9) on the following form:

$$\begin{aligned} \partial_t m_k + \partial_x f_k &= 0, \\ \partial_t I_k + \partial_x g_k + \alpha_k \partial_x p + (\Delta p)\partial_x \alpha_k &= Q_k, \end{aligned} \tag{41}$$

where $k = \mathrm{g}, \mathrm{l}$ and

$$\begin{aligned} f_k &= \rho_k \alpha_k v_k \quad \text{and} \quad m_k = \rho_k \alpha_k \\ g_k &= \rho_k \alpha_k v_k^2 \quad \text{and} \quad I_k = \rho_k \alpha_k v_k. \end{aligned}$$

We assume that we have given approximations $\left(m^n_{k,j}, I^n_{k,j}\right) \approx \left(m_{k,j}(t^n), I_{k,j}(t^n)\right)$. Approximations $m_{k,j}(t)$ and $I_{k,j}(t)$ for $t \in (t^n, t^{n+1}]$ are now constructed by solving the following ODE problem:

$$\begin{aligned} \dot{m}_{k,j} + \delta_x F_{k,j} &= 0, \\ \dot{I}_{k,j} + \delta_x G_{k,j} + \alpha_{k,j}\delta_x P_j + (\Delta p)_j \delta_x \Lambda_{k,j} &= Q_{k,j}, \end{aligned} \tag{42}$$

subject to the initial conditions

$$m_{k,j}(t^n) = m^n_{k,j}, \qquad I_{k,j}(t^n) = I^n_{k,j}.$$

Here δ_x is the operator defined by

$$\delta_x w_j = \frac{w_{j+1/2} - w_{j-1/2}}{\Delta x}, \qquad \delta_x w_{j+1/2} = \frac{w_{j+1} - w_j}{\Delta x},$$

and $(\Delta p)_j(t) = (\Delta p)\,(U_j(t), \delta)$ is obtained from (16). Moreover, $F_{k,j+1/2}(t) = F_k(U_j(t), U_{j+1}(t))$, $G_{k,j+1/2}(t) = G_k(U_j(t), U_{j+1}(t))$, $P_{j+1/2}(t) = P(U_j(t), U_{j+1}(t))$, and $\Lambda_{k,j+1/2}(t) = \Lambda_k(U_j(t), U_{j+1}(t))$ are assumed to be numerical fluxes consistent with the corresponding physical fluxes, i.e.

$$\begin{aligned} F_k(U,U) &= f_k = \rho_k \alpha_k v_k \\ G_k(U,U) &= g_k = \rho_k \alpha_k v_k^2 \\ P(U,U) &= p \\ \Lambda_k(U,U) &= \alpha_k. \end{aligned}$$

4.2. **The class of Mixture Flux (MF) methods.** Before we describe the MF approach it will be useful to introduce some basic concepts consistent with those used in [11, 12]. Assume that we consider a contact discontinuity given by

$$\begin{aligned} p_{\mathrm{L}} = p_{\mathrm{R}} &= p \\ \alpha_{\mathrm{L}} &\neq \alpha_{\mathrm{R}} \\ (v_{\mathrm{g}})_{\mathrm{L}} = (v_{\mathrm{l}})_{\mathrm{L}} = (v_{\mathrm{g}})_{\mathrm{R}} &= (v_{\mathrm{l}})_{\mathrm{R}} = v, \end{aligned} \tag{43}$$

for the time period $[t^n, t^{n+1}]$. All pressure terms vanish from the model (6)-(9), and it is seen that the solution to this initial value problem is simply that the discontinuity will propagate with the velocity v. The exact solution of the Riemann problem will then give the numerical mass flux

$$(\rho\alpha v)_{j+1/2} = \frac{1}{2}\rho(\alpha_{\mathrm{L}} + \alpha_{\mathrm{R}})v - \frac{1}{2}\rho(\alpha_{\mathrm{R}} - \alpha_{\mathrm{L}})|v|. \tag{44}$$

Definition 3. *A numerical flux F that satisfies (44) for the contact discontinuity (43) will in the following be termed a "mass coherent" flux.*

Definition 4. *A pair of numerical fluxes $(F_{\mathrm{l}}, F_{\mathrm{g}})$ that satisfy the relation*

$$\rho_{\mathrm{g}} F_{\mathrm{l},j+1/2} + \rho_{\mathrm{l}} F_{\mathrm{g},j+1/2} = \rho_{\mathrm{g}}\rho_{\mathrm{l}} v. \tag{45}$$

for the contact discontinuity (43) will in the following be termed "pressure coherent" fluxes.

For a more detailed presentation of the motivation behind these definitions we refer to [12, 11]. With these definitions in hand we can proceed to a more precise definition of the Mixture Flux methods.

Definition 5. *We will use the term* **Mixture Flux** *(MF) methods to denote numerical algorithms which are constructed within the semidiscrete frame of* (42) *where fluxes are given as follows:*

(1) *The numerical flux $\Lambda_{k,j+1/2}(t)$ is obtained as*

$$\Lambda_{k,j+1/2}(t) = \frac{\alpha_{k,j}(t) + \alpha_{k,j+1}(t)}{2}. \tag{46}$$

(2) *We determine $P_{j+1/2}(t)$ for $t \in (t^n, t^{n+1}]$ by solving the ODE*

$$\begin{aligned} &\dot{P}_{j+1/2} + [\kappa_{j+1/2}\rho_{\mathrm{l},j+1/2}]\delta_x I_{\mathrm{g},j+1/2} + [\kappa_{j+1/2}\rho_{\mathrm{g},j+1/2}]\delta_x I_{\mathrm{l},j+1/2} = 0 \\ &P_{j+1/2}(t_+^n) = \frac{p_j^n + p_{j+1}^n}{2}, \end{aligned} \tag{47}$$

where the interface values $\kappa_{j+1/2}$ and $\rho_{k,j+1/2}$ are computed from $P_{j+1/2}(t)$ together with the arithmetic average (46) *which defines $\alpha_{k,j+1/2}(t)$. Here κ is given by*

$$\kappa = \frac{1}{\frac{\partial\rho_{\mathrm{l}}}{\partial p}\alpha_{\mathrm{l}}\rho_{\mathrm{g}} + \frac{\partial\rho_{\mathrm{g}}}{\partial p}\alpha_{\mathrm{g}}\rho_{\mathrm{l}}}. \tag{48}$$

(3) *We consider hybrid mass fluxes* $F_{k,j+1/2}(t)$ *of the form*

$$F_{\mathrm{l},j+1/2}(t) = \kappa_{j+1/2}(t)\left(\rho_{\mathrm{g}}\alpha_{\mathrm{l}}\frac{\partial\rho_{\mathrm{l}}}{\partial p}F_{\mathrm{l}}^{\mathrm{D}}(t) + \rho_{\mathrm{l}}\alpha_{\mathrm{g}}\frac{\partial\rho_{\mathrm{g}}}{\partial p}F_{\mathrm{l}}^{\mathrm{A}}(t) + \rho_{\mathrm{l}}\alpha_{\mathrm{l}}\frac{\partial\rho_{\mathrm{l}}}{\partial p}(F_{\mathrm{g}}^{\mathrm{D}} - F_{\mathrm{g}}^{\mathrm{A}})(t)\right)_{j+1/2} \tag{49}$$

and

$$F_{\mathrm{g},j+1/2}(t) = \kappa_{j+1/2}(t)\left(\rho_{\mathrm{l}}\alpha_{\mathrm{g}}\frac{\partial\rho_{\mathrm{g}}}{\partial p}F_{\mathrm{g}}^{\mathrm{D}}(t) + \rho_{\mathrm{g}}\alpha_{\mathrm{l}}\frac{\partial\rho_{\mathrm{l}}}{\partial p}F_{\mathrm{g}}^{\mathrm{A}}(t) + \rho_{\mathrm{g}}\alpha_{\mathrm{g}}\frac{\partial\rho_{\mathrm{g}}}{\partial p}(F_{\mathrm{l}}^{\mathrm{D}} - F_{\mathrm{l}}^{\mathrm{A}})(t)\right)_{j+1/2}. \tag{50}$$

The coefficient variables at $j+1/2$ *are determined from the cell interface pressure* $P_{j+1/2}(t)$ *as well as the relation*

$$\alpha_{j+1/2}(t) = \frac{1}{2}(\alpha_j(t) + \alpha_{j+1}(t))$$

which is consistent with the treatment of the coefficients of the pressure evolution equation (47).

(a) *The flux component* $F_k^{\mathrm{A}}(t)$ *is assumed to be consistent with its physical flux* $(\rho\alpha v)_k(t)$ *as well as "mass coherent" in the sense of Definition 3.*
(b) *The flux component* $F_k^{\mathrm{D}}(t)$ *is assumed to be consistent with its physical flux* $(\rho\alpha v)_k(t)$ *as well as "pressure coherent" in the sense of Definition 4.*

(4) *We choose* $G_{k,j+1/2}(t)$ *to be consistent with the flux component* $F_{k,j+1/2}^{\mathrm{A}}(t)$ *in the following sense: For a flow with velocities which are constant in space for the time interval* $[t^n, t^{n+1}]$, *that is,*

$$v_{k,j}(t) = v_{k,j+1}(t) = v_k(t), \qquad t \in [t^n, t^{n+1}], \tag{51}$$

we assume that $G_{k,j+1/2}(t)$ *takes the form*

$$G_{k,j+1/2}(t) = G_{k,j+1/2}^{\mathrm{A}}(t) = v_k(t)F_{k,j+1/2}^{\mathrm{A}}(t), \tag{52}$$

where $F_{k,j+1/2}^{\mathrm{A}}(t)$ *is the numerical flux component introduced above.*

It is easy to check that the above numerical fluxes $\Lambda_{k,j+1/2}$, $P_{j+1/2}$, $F_{k,j+1/2}$, and $G_{k,j+1/2}$ are consistent with the corresponding physical fluxes. We refer to [12] for more details. We now state the following important lemma whose proof can also be found in [12]:

Lemma 1. *Let the mixture fluxes (49) and (50) be constructed from pressure coherent fluxes* F_k^{D} *in the sense of Definition 4, and mass coherent fluxes* F_k^{A} *in the sense of Definition 3. Then the hybrid fluxes (49) and (50) reduce to the upwind fluxes (44) on the contact discontinuity (43), i.e. they are mass coherent.*

It follows directly from Definition 5 and Lemma 1 that

Corollary 1. *The mass fluxes of the MF methods given by Definition 5, are mass coherent in the sense of Definition 3.*

Moreover, by application of Lemma 1 and Definition 5, we can verify that the MF methods satisfy the following principle due to Abgrall [1, 21, 22]:
A flow, uniform in pressure and velocity must remain uniform in the same variables during its time evolution. We refer to [12] for its straightforward proof.

Corollary 2. *The MF methods given by Definition 5, obey Abgrall's principle. More precisely, for the contact discontinuity* (43) *the semidiscrete approximation* (42) *takes the following form*

$$\begin{aligned} \dot{m}_{k,j} + \delta_x(\rho_k\alpha_k v_k)_j &= 0, \\ v\,\dot{m}_{k,j} + v\delta_x(\rho_k\alpha_k v_k)_j &= 0, \end{aligned} \tag{53}$$

where $(\rho_k\alpha_k v_k)_{j+1/2}$ *is on the form* (44). *Consequently, no momentum change is introduced and the contact discontinuity remains unchanged except from experiencing a convective transport.*

In conclusion, Corollary 1 states that the MF mass fluxes recover the numerical fluxes of an exact Riemann solver for a moving or stationary contact discontinuity. Corollary 2 ensures that Abgrall's principle [1] is satisfied. The fact that this principle is obeyed, ensures that the use of the pressure evolution equation (47) in the discretization of the non-conservative pressure term is consistent with basic physical understanding of two-phase flow phenomena.

Remark 3 (Mixture mass fluxes). *The following differential relations are obtained from the basic relation* (17) *(see* [12, 11] *for more details):*

$$\begin{aligned} dp &= \kappa(\rho_{\mathrm{l}} dm_{\mathrm{g}} + \rho_{\mathrm{g}} dm_{\mathrm{l}}) \\ d\alpha_{\mathrm{l}} &= \kappa(-\frac{\partial \rho_{\mathrm{l}}}{\partial p}\alpha_{\mathrm{l}} dm_{\mathrm{g}} + \frac{\partial \rho_{\mathrm{g}}}{\partial p}\alpha_{\mathrm{g}} dm_{\mathrm{l}}), \end{aligned} \tag{54}$$

where κ *is given by* (48) *and*

$$\begin{aligned} dm_{\mathrm{g}} &= \alpha_{\mathrm{g}}\frac{\partial \rho_{\mathrm{g}}}{\partial p} dp - \rho_{\mathrm{g}} d\alpha_{\mathrm{l}} \\ dm_{\mathrm{l}} &= \alpha_{\mathrm{l}}\frac{\partial \rho_{\mathrm{l}}}{\partial p} dp + \rho_{\mathrm{l}} d\alpha_{\mathrm{l}}. \end{aligned} \tag{55}$$

The mixture mass fluxes (49) *and* (50) *are obtained by first introducing a flux component* F_p *(associated with the pressure) and* F_α *(associated with the volume fraction) such that the mass fluxes* F_{l} *and* F_{g}*, inspired by* (55)*, are given by*

$$\begin{aligned} F_{\mathrm{l}} &= \alpha_{\mathrm{l}}\frac{\partial \rho_{\mathrm{l}}}{\partial p} F_p + \rho_{\mathrm{l}} F_\alpha \\ F_{\mathrm{g}} &= \alpha_{\mathrm{g}}\frac{\partial \rho_{\mathrm{g}}}{\partial p} F_p - \rho_{\mathrm{g}} F_\alpha. \end{aligned} \tag{56}$$

Inspired by the differential relations (54) *we propose to give* F_p *and* F_α *the following form*

$$\begin{aligned} F_p &= \kappa\rho_{\mathrm{g}} F_{\mathrm{l}}^{\mathrm{D}} + \kappa\rho_{\mathrm{l}} F_{\mathrm{g}}^{\mathrm{D}} \\ F_\alpha &= \kappa\frac{\partial \rho_{\mathrm{g}}}{\partial p}\alpha_{\mathrm{g}} F_{\mathrm{l}}^{\mathrm{A}} - \kappa\frac{\partial \rho_{\mathrm{l}}}{\partial p}\alpha_{\mathrm{l}} F_{\mathrm{g}}^{\mathrm{A}}, \end{aligned} \tag{57}$$

where $F_{\mathrm{k}}^{\mathrm{D}}$ *should possess the "pressure coherency" property whereas* $F_{\mathrm{k}}^{\mathrm{A}}$ *should possess the "mass coherency" property. Combining* (56) *and* (57) *yields the mixture mass fluxes* (49) *and* (50)*. The purpose of the* $F_{\mathrm{k}}^{\mathrm{D}}$ *component is to ensure that stable (non-oscillatory) pressure calculations based on* (17) *is obtained whereas the purpose of the* $F_{\mathrm{k}}^{\mathrm{A}}$ *component is to ensure accurate resolution of volume fraction contact discontinuities.*

Remark 4 (Pressure evolution equation). *Since the pressure calculation is based on the masses* m_k *through the relation* (17)*, we want the pressure* p *to be consistent with the mass equations*

$$\partial_t m_k + \partial_x f_k = 0. \tag{58}$$

This equation can be recast in terms of the pressure variable as follows: Multiplying the gas mass conservation equation by $\kappa\rho_{\mathrm{l}}$ *and the liquid mass conservation equation by* $\kappa\rho_{\mathrm{g}}$ *and then adding the two resulting equations, yields the equation*

$$\kappa\rho_{\mathrm{l}}\frac{\partial}{\partial t} m_{\mathrm{g}} + \kappa\rho_{\mathrm{g}}\frac{\partial}{\partial t} m_{\mathrm{l}} + \kappa\rho_{\mathrm{l}}\frac{\partial}{\partial x}\left(\rho_{\mathrm{g}}\alpha_{\mathrm{g}} v_{\mathrm{g}}\right) + \kappa\rho_{\mathrm{g}}\frac{\partial}{\partial x}\left(\rho_{\mathrm{l}}\alpha_{\mathrm{l}} v_{\mathrm{l}}\right) = 0.$$

In view of the first relation of (54)*, the following pressure evolution equation is obtained*

$$\partial_t p + \kappa\rho_{\mathrm{l}}\partial_x I_{\mathrm{g}} + \kappa\rho_{\mathrm{g}}\partial_x I_{\mathrm{l}} = 0.$$

We want to consider a discretization of this equation at the cell interface in order to obtain an appropriate numerical pressure flux $P_{j+1/2}(t)$ *for* $t \in (t^n, t^{n+1}]$*. This is the motivation leading to* (47)*.*

Remark 5 (The mass flux F_k^{D}). *The mass flux component F_k^{D} is associated with the pressure calculation as described in Remark 3. Therfore it is natural to choose a discretization of this flux which is consistent with the discretization of the pressure evolution equation. On the semi-discrete level, in view of* (47)*, we therefore propose to consider the following discretization of the mass conservation equation* (58)

$$\begin{aligned} \dot{m}_{k,j+1/2} + \delta_x I_{k,j+1/2} &= 0, \qquad t \in (t^n, t^{n+1}] \\ m_{k,j+1/2}(t_+^n) &= \frac{m_{k,j}^n + m_{k,j+1}^n}{2}. \end{aligned} \tag{59}$$

We now suggest to average as follows:

$$m_{k,j}(t) = \frac{1}{2}\left(m_{k,j-1/2}(t) + m_{k,j+1/2}(t)\right),$$

which implies that

$$\dot{m}_{k,j}\,(t) = \frac{1}{2}\left(\dot{m}_{k,j-1/2}\,(t) + \dot{m}_{k,j+1/2}\,(t)\right). \tag{60}$$

By substituting (59) *into* (60) *we obtain the following ODE equation for $m_{k,j}(t)$:*

$$\begin{aligned} \dot{m}_{k,j} + \frac{1}{2\Delta x}(I_{k,j+1} - I_{k,j-1}) &= 0, \qquad t \in (t^n, t^{n+1}] \\ m_{k,j}(t_+^n) &= \frac{1}{4}\Big(m_{k,j-1}^n + 2m_{k,j}^n + m_{k,j+1}^n\Big). \end{aligned}$$

This equation is the basis for designing the flux component $F_{k,j+1/2}^{\mathrm{D}}$.

5. Three fully discrete MF schemes

The purpose of this section is to construct fully discrete schemes based on the general class of MF schemes given by Definition 5. We first describe how to construct appropriate candidates for the mass flux components F_k^{A} and F_k^{D} which were introduced in Definition 5. Then we apply these components to propose fully discrete schemes, denoted respectively as *MF-AUSM$^+$*, *MF-CVS*, and *MF-AUSMD*. The difference between them lies in the choice of the convective fluxes only, that is, the F_k^{A} and G_k^{A} components.

5.1. A pressure coherent convective mass flux F_k^{D}.

As explained in Remark 5 we shall define the numerical flux F_k^{D} from the following ODE equation for $m_{k,j}(t)$:

$$\begin{aligned} \dot{m}_{k,j} + \frac{1}{2\Delta x}(I_{k,j+1} - I_{k,j-1}) &= 0, \qquad t \in (t^n, t^{n+1}] \\ m_{k,j}(t_+^n) &= \frac{1}{4}\Big(m_{k,j-1}^n + 2m_{k,j}^n + m_{k,j+1}^n\Big). \end{aligned} \tag{61}$$

A fully discrete version of (61) is given by

$$\frac{m_{k,j}^{n+1} - \frac{1}{4}\left(2m_{k,j}^n + m_{k,j-1}^n + m_{k,j+1}^n\right)}{\Delta t} + \frac{1}{2\Delta x}\left(I_{k,j+1}^n - I_{k,j-1}^n\right) = 0. \tag{62}$$

This equation can be written on the flux-conservative form

$$m_{k,j}^{n+1} = m_{k,j}^n - \Delta t \delta_x F_{k,j}^{\mathrm{D},n},$$

where

$$F_{k,j+1/2}^{\mathrm{D},n} = \frac{1}{2}(I_{k,j}^n + I_{k,j+1}^n) + \frac{1}{4}\frac{\Delta x}{\Delta t}(m_{k,j}^n - m_{k,j+1}^n). \tag{63}$$

We can easily check that the proposed flux F_k^{D} possesses the "pressure coherent" property of Definition 4, see [12, 11].

Proposition 1. *The flux component F_k^{D} given by* (63) *is pressure coherent in the sense of Definition 4.*

5.2. Convective fluxes F_k^{A} and G_k^{A}.

5.2.1. *Van Leer.* Our starting point is a simpler (lower order) version of the splitting formulas (26) used in the AUSM$^+$ scheme

$$V^{\pm}(v,c) = \begin{cases} \pm\frac{1}{4c}(v \pm c)^2 & \text{if } |v| \leq c \\ \frac{1}{2}(v \pm |v|) & \text{otherwise.} \end{cases} \tag{64}$$

We now let the numerical fluxes be given as follows:

(1) *Mass Flux.* We let the numerical mass flux $(\rho\alpha v)_{j+1/2}$ be given as

$$(\rho\alpha v)_{j+1/2} = (\rho\alpha)_{\mathrm{L}} V^{+}(v_{\mathrm{L}}, c_{j+1/2}) + (\rho\alpha)_{\mathrm{R}} V^{-}(v_{\mathrm{R}}, c_{j+1/2}) \tag{65}$$

for each phase.

(2) *Momentum Flux.* We let the numerical convective momentum flux $(\rho\alpha v^2)_{j+1/2}$ be defined by employing upwinding based on the cell interface momentum $(\rho\alpha v)_{j+1/2}$

$$(\rho\alpha v^2)_{j+1/2} = \begin{cases} (\rho\alpha v)_{j+1/2} v_{\mathrm{L}} & \text{if } (\rho\alpha v)_{j+1/2} \geq 0 \\ (\rho\alpha v)_{j+1/2} v_{\mathrm{R}} & \text{otherwise.} \end{cases} \tag{66}$$

The van Leer fluxes possess good stability properties but are excessively diffusive on the volume fraction waves. This motivates for proposing a mechanism for eliminating numerical dissipation, along the lines of Wada and Liou [28].

5.2.2. *AUSMD.* We consider the AUSMD scheme [10] obtained by replacing the splitting formulas $V^{\pm}$ in the van Leer scheme with the less diffusive pair

$$\tilde{V}^{\pm}(v,c,\chi) = \begin{cases} \chi V^{\pm}(v,c) + (1-\chi)\frac{v \pm |v|}{2} & |v| < c \\ \frac{1}{2}(v \pm |v|) & \text{otherwise} \end{cases} \tag{67}$$

where

$$\chi_{\mathrm{L}} = \frac{2(\rho/\alpha)_{\mathrm{L}}}{(\rho/\alpha)_{\mathrm{L}} + (\rho/\alpha)_{\mathrm{R}}} \tag{68}$$

and

$$\chi_{\mathrm{R}} = \frac{2(\rho/\alpha)_{\mathrm{R}}}{(\rho/\alpha)_{\mathrm{L}} + (\rho/\alpha)_{\mathrm{R}}} \tag{69}$$

for each phase. That is,

(1) *Mass Flux.*

$$(\rho\alpha v)_{j+1/2} = (\rho\alpha)_{\mathrm{L}} \tilde{V}^{+}(v_{\mathrm{L}}, c_{j+1/2}, \chi_{\mathrm{L}}) + (\rho\alpha)_{\mathrm{R}} \tilde{V}^{-}(v_{\mathrm{R}}, c_{j+1/2}, \chi_{\mathrm{R}}) \tag{70}$$

for each phase.

(2) *Momentum Flux.*

$$(\rho\alpha v^2)_{j+1/2} = \begin{cases} (\rho\alpha v)_{j+1/2} v_{\mathrm{L}} & \text{if } (\rho\alpha v)_{j+1/2} \geq 0 \\ (\rho\alpha v)_{j+1/2} v_{\mathrm{R}} & \text{otherwise.} \end{cases} \tag{71}$$

We remark that for the van Leer and AUSMD schemes, it is essential to use a common velocity of sound to both phases to avoid oscillations in the pressure variable. We refer to [10, 12] for details. Here we use the mixture sound velocity given by (21), and define

$$c_{j+1/2} = \max(c_j, c_{j+1}). \tag{72}$$

5.2.3. *AUSM$^+$.* We define a cell interface velocity $v_{j+1/2}$ as

$$v_{j+1/2} = V^{+}(v_{\mathrm{L}}, c_{j+1/2}) + V^{-}(v_{\mathrm{R}}, c_{j+1/2}), \tag{73}$$

where the splitting functions $V^{\pm}$ now are given by (26) and obtain the convective fluxes as follows:

(1) *Mass Flux.*

$$(\rho\alpha v)_{j+1/2} = \begin{cases} (\rho\alpha)_{\mathrm{L}} v_{j+1/2} & \text{if } v_{j+1/2} \geq 0 \\ (\rho\alpha)_{\mathrm{R}} v_{j+1/2} & \text{otherwise} \end{cases} \tag{74}$$

(2) *Momentum Flux.*

$$(\rho\alpha v^2)_{j+1/2} = \begin{cases} (\rho\alpha v)_{\mathrm{L}} v_{j+1/2} & \text{if } v_{j+1/2} \geq 0 \\ (\rho\alpha v)_{\mathrm{R}} v_{j+1/2} & \text{otherwise.} \end{cases} \tag{75}$$

5.2.4. *CVS.* We define a cell interface velocity $v_{j+1/2}$ as

$$v_{j+1/2} = \frac{1}{2}(v_{\rm L} + |v_{\rm L}|) + \frac{1}{2}(v_{\rm R} - |v_{\rm R}|). \tag{76}$$

This corresponds to (73) with $V^{\pm}$ chosen as

$$V^{\pm}(v, c) = \frac{1}{2}(v \pm |v|).$$

Then we obtain convective fluxes as for the AUSM$^+$ scheme described by (74) and (75). Hence, the upwinding in CVS is based on pure advection. In particular, CVS does not make use of a numerical sound velocity to determine the upwind direction.

In the following we use AUSMD, AUSM$^+$, and CVS convective fluxes as bases to define MF type of schemes. In this connection it is relevant to note that AUSMD, AUSM$^+$, and CVS mass fluxes possess the "mass coherent" property.

Proposition 2. *The convective fluxes* $(\rho\alpha v)^{\rm AUSMD}_{j+1/2}$, $(\rho\alpha v)^{\rm AUSM^+}_{j+1/2}$, *and* $(\rho\alpha v)^{\rm CVS}_{j+1/2}$ *are mass coherent in the sense of Definition 3.*

5.3. **Three Mixture Flux (MF) Schemes.** We are now ready to describe fully discrete MF schemes.

5.3.1. *General form.* We use the shorthands $m_k = \rho_k\alpha_k$ and $I_k = m_k v_k$ and consider a fully discrete scheme based on (42) given as follows.

- Gas Mass
$$\frac{m^{n+1}_{{\rm g},j} - m^n_{{\rm g},j}}{\Delta t} = -\delta_x F^n_{{\rm g},j} \tag{77}$$
- Liquid Mass
$$\frac{m^{n+1}_{{\rm l},j} - m^n_{{\rm l},j}}{\Delta t} = -\delta_x F^n_{{\rm l},j} \tag{78}$$
- Gas Momentum
$$\begin{aligned}&\frac{I^{n+1}_{{\rm g},j} - I^n_{{\rm g},j}}{\Delta t}\\ &= -\delta_x G^{{\rm A},n}_{{\rm g},j} - \alpha^n_{{\rm g},j}\delta_x P^{n+1}_j - (\Delta p)^n_j \delta_x \Lambda^n_{{\rm g},j} + (Q_{\rm g})^n_j.\end{aligned} \tag{79}$$
- Liquid Momentum
$$\begin{aligned}&\frac{I^{n+1}_{{\rm l},j} - I^n_{{\rm l},j}}{\Delta t}\\ &= -\delta_x G^{{\rm A},n}_{{\rm l},j} - \alpha^n_{{\rm l},j}\delta_x P^{n+1}_j - (\Delta p)^n_j \delta_x \Lambda^n_{{\rm l},j} + (Q_{\rm l})^n_j.\end{aligned} \tag{80}$$

5.3.2. *MF-AUSMD.*

Definition 6. *We will use the term* **MF-AUSMD** *to denote the numerical algorithm which is constructed within the discrete frame of* (77)–(80) *where fluxes are given as follows:*

(1) *The numerical flux* $\Lambda^n_{k,j+1/2}$ *is obtained as*
$$\Lambda^n_{k,j+1/2} = \frac{\alpha^n_{k,j} + \alpha^n_{k,j+1}}{2}. \tag{81}$$

(2) *We determine* $P^{n+1}_{j+1/2}$ *by considering the following discretization of the pressure evolution equation* (47)
$$\begin{aligned}&\frac{P^{n+1}_{j+1/2} - \frac{1}{2}(p^n_j + p^n_{j+1})}{\Delta t}\\ &= -(\kappa\rho_{\rm l})^n_{j+1/2}\frac{I^n_{{\rm g},j+1} - I^n_{{\rm g},j}}{\Delta x} - (\kappa\rho_{\rm g})^n_{j+1/2}\frac{I^n_{{\rm l},j+1} - I^n_{{\rm l},j}}{\Delta x},\end{aligned} \tag{82}$$
where the interface values $\kappa^n_{j+1/2}$ *and* $\rho^n_{k,j+1/2}$ *are computed from* $P^n_{j+1/2}$ *together with the arithmetic average* (81) *which defines* $\alpha^n_{k,j+1/2}$.

(3) *We consider hybrid mass fluxes* $F^n_{k,j+1/2}$ *of the form*

$$F^n_{\mathrm{l},j+1/2} = \Big([\kappa\rho_{\mathrm{g}}\alpha_{\mathrm{l}}\partial_p\rho_{\mathrm{l}}]^n F^{\mathrm{D},n}_{\mathrm{l}} + [\kappa\rho_{\mathrm{l}}\alpha_{\mathrm{g}}\partial_p\rho_{\mathrm{g}}]^n F^{\mathrm{A},n}_{\mathrm{l}} + [\kappa\rho_{\mathrm{l}}\alpha_{\mathrm{l}}\partial_p\rho_{\mathrm{l}}]^n (F^{\mathrm{D},n}_{\mathrm{g}} - F^{\mathrm{A},n}_{\mathrm{g}})\Big)_{j+1/2} \tag{83}$$

and

$$F^n_{\mathrm{g},j+1/2} = \Big([\kappa\rho_{\mathrm{l}}\alpha_{\mathrm{g}}\partial_p\rho_{\mathrm{g}}]^n F^{\mathrm{D},n}_{\mathrm{g}} + [\kappa\rho_{\mathrm{g}}\alpha_{\mathrm{l}}\partial_p\rho_{\mathrm{l}}]^n F^{\mathrm{A},n}_{\mathrm{g}} + [\kappa\rho_{\mathrm{g}}\alpha_{\mathrm{g}}\partial_p\rho_{\mathrm{g}}]^n (F^{\mathrm{D},n}_{\mathrm{l}} - F^{\mathrm{A},n}_{\mathrm{l}})\Big)_{j+1/2}. \tag{84}$$

The coefficient variables at $j+1/2$ *are determined from the cell interface pressure* $P^n_{j+1/2}$ *as well as the relation*

$$\alpha^n_{j+1/2} = \frac{1}{2}(\alpha^n_j + \alpha^n_{j+1})$$

which is consistent with the treatment of the coefficients of the pressure evolution equation (82).

(a) *For the flux component* $F^{\mathrm{A},n}_{k,j+1/2}$ *we refer to Section 5.2 and use*

$$F^{\mathrm{A},n}_{k,j+1/2} = (\rho\alpha v)^{\mathrm{AUSMD},n}_{k,j+1/2}. \tag{85}$$

(b) *For the flux component* $F^{\mathrm{D},n}_{k,j+1/2}$ *we refer to Section 5.1 and use*

$$F^{\mathrm{D},n}_{k,j+1/2} = \frac{1}{2}(I^n_{k,j} + I^n_{k,j+1}) + \frac{1}{4}\frac{\Delta x}{\Delta t}(m^n_{k,j} - m^n_{k,j+1}). \tag{86}$$

(4) *The flux component* $G^n_{k,j+1/2}$ *is chosen to be consistent with the flux component* $F^{\mathrm{A},n}_{k,j+1/2}$ *by using*

$$G^n_{k,j+1/2} = G^{\mathrm{A},n}_{k,j+1/2} = (\rho\alpha v^2)^{\mathrm{AUSMD},n}_{k,j+1/2}. \tag{87}$$

Definition 7. *We will use the term* **MF-AUSM$^+$** *to denote the numerical algorithm which is identical to* **MF-AUSMD** *except from the convective flux terms* $F^{\mathrm{A},n}_{k,j+1/2}$ *and* $G^{\mathrm{A},n}_{k,j+1/2}$ *which are defined as follows:*

(a) *For the flux component* $F^{\mathrm{A},n}_{k,j+1/2}$ *we use*

$$F^{\mathrm{A},n}_{k,j+1/2} = (\rho\alpha v)^{\mathrm{AUSM}^+,n}_{k,j+1/2}. \tag{88}$$

(b) *For the flux component* $G^{\mathrm{A},n}_{k,j+1/2}$ *we use*

$$G^{\mathrm{A},n}_{k,j+1/2} = (\rho\alpha v^2)^{\mathrm{AUSM}^+,n}_{k,j+1/2}. \tag{89}$$

Definition 8. *We will use the term* **MF-CVS** *to denote the numerical algorithm which is identical to* **MF-AUSM** *except from the convective flux terms* $F^{\mathrm{A},n}_{k,j+1/2}$ *and* $G^{\mathrm{A},n}_{k,j+1/2}$ *which are defined as follows:*

(a) *For the flux component* $F^{\mathrm{A},n}_{k,j+1/2}$ *we use*

$$F^{\mathrm{A},n}_{k,j+1/2} = (\rho\alpha v)^{\mathrm{CVS},n}_{k,j+1/2}. \tag{90}$$

(b) *For the flux component* $G^{\mathrm{A},n}_{k,j+1/2}$ *we use*

$$G^{\mathrm{A},n}_{k,j+1/2} = (\rho\alpha v^2)^{\mathrm{CVS},n}_{k,j+1/2}. \tag{91}$$

In view of Definitions 6, 7, and 8 and Proposition 1 and Proposition 2 it follows that MF-AUSMD, MF-AUSM$^+$, and MF-CVS are MF schemes in the sense of Definition 5. Consequently, Corollary 1 and 2 are applicable, and we immediately conclude that

Proposition 3. *MF-AUSMD, MF-AUSM$^+$, and MF-CVS satisfy the following properties: (i) The mass fluxes are mass coherent in the sense of Definition 3. (ii) All schemes obey Abgrall's principle.*

6. Viscosity Rescaling

6.1. **Motivation.** Although the MF class of schemes allows for excellent accuracy and robustness, it is observed that a timestep stability criterion applies that is more strict than the standard CFL criterion

$$\frac{\Delta x}{\Delta t} \geq |\lambda|_{\max}. \tag{92}$$

To shed some light on the mechanism behind this feature, we write (63) as

$$F^{\mathrm{D},n}_{k,j+1/2} = F^{\mathrm{D}}_k(U^n_j, U^n_{j+1}) = \frac{1}{2}(I^n_{k,j} + I^n_{k,j+1}) + \frac{1}{2}\frac{\Delta x}{\Delta t}\mathcal{D}^n_{j+1/2}(m^n_{k,j} - m^n_{k,j+1}), \tag{93}$$

where the numerical viscosity coefficient is simply $\mathcal{D}^n_{j+1/2} = 1/2$. Assuming that the pressure waves travel with the velocity of sound c (i.e. assuming $v_k << c$), the following stability criterion applies [24]

$$c\frac{\Delta t}{\Delta x} \leq \mathcal{D}^n_{j+1/2} \leq 1, \tag{94}$$

where we consider the mass equation as an independent, scalar equation. Hence, using the value $\mathcal{D}_{j+1/2} = 1/2$ we obtain the CFL-like criterion

$$\frac{\Delta x}{\Delta t} \geq 2c, \tag{95}$$

which is twice as strict as the expected

$$\frac{\Delta x}{\Delta t} \geq c. \tag{96}$$

Here the mass equations are viewed as scalar equations and stabilizing effects related to couplings between the other equations are not taken into account. However, this simple analysis may to a large extent explain why a restrictive stability criterion applies for the explicit (in time) MF class of schemes.

6.2. **Rescaled MF schemes.** To improve matters, we suggest scaling the numerical viscosity of the flux (63) as follows

$$F^{\mathrm{D},n}_{k,j+1/2} = F^{\mathrm{D}}_k(U^n_j, U^n_{j+1}) = \frac{1}{2}(I^n_{k,j} + I^n_{k,j+1}) + \frac{1}{4}\psi^n_{j+1/2}\frac{\Delta x}{\Delta t}(m^n_{k,j} - m^n_{k,j+1}), \tag{97}$$

where

$$\psi^n_{j+1/2} = 2c^n_{j+1/2}\frac{\Delta t}{\Delta x}. \tag{98}$$

Here we use the mathematical mixture sound velocity (21) to define $c^n_{j+1/2}$.

The choice (98) ensures that the numerical viscosity behaves as an upwind viscosity for a wave which travels with the velocity c. That is, assuming that $|v^n_{k,j}| = |v^n_{k,j+1}| = |v^n_{k,j+1/2}| = c^n_{j+1/2}$ we see that $F^{\mathrm{D},n}_{k,j+1/2}$ takes the form

$$F^{\mathrm{D},n}_{k,j+1/2} = \begin{cases} m^n_{k,j}v^n_{k,j+1/2} & \text{if } v^n_{k,j+1/2} \geq 0 \\ m^n_{k,j+1}v^n_{k,j+1/2} & \text{otherwise.} \end{cases} \tag{99}$$

In view of (93) and (94) we see that the stability condition now reads

$$\frac{\psi^n_{j+1/2}}{2} \leq 1,$$

which is in accordance with the standard CFL criterion (96).

The interplay between the pressure evolution equation and the F^{D} flux suggests that we should also rescale the viscosity for the cell interface pressure (82). We modify as follows:

$$p^{n+1}_{j+1/2} = \frac{1}{2}\left(p^n_j + p^n_{j+1}\right) + \xi^n_{j+1/2}\frac{\Delta t}{\Delta x}\Big[D^n_{\mathrm{g},j+1/2}(I^n_{\mathrm{g},j} - I^n_{\mathrm{g},j+1}) + D^n_{\mathrm{l},j+1/2}(I^n_{\mathrm{l},j} - I^n_{\mathrm{l},j+1})\Big], \tag{100}$$

where $D^n_{\mathrm{g},j+1/2} = (\kappa\rho_{\mathrm{l}})^n_{j+1/2}$ and $D^n_{\mathrm{l},j+1/2} = (\kappa\rho_{\mathrm{g}})^n_{j+1/2}$.

To determine $\xi^n_{j+1/2}$ we consider the model equation

$$\frac{\partial u}{\partial t} + c\frac{\partial u}{\partial x} = 0, \tag{101}$$

which describes advection of u with the velocity $c > 0$. Discretizing (101) at the cell interfaces with a staggered Lax-Friedrichs scheme, similar to (100), we obtain

$$u^{n+1}_{j+1/2} = \frac{1}{2}\left(u^n_j + u^n_{j+1}\right) + \xi^n_{j+1/2} c^n_{j+1/2}\frac{\Delta t}{\Delta x}\left(u^n_j - u^n_{j+1}\right) \tag{102}$$

Treating $u^{n+1}_{j+1/2}$ as a flux, we wish to recover the upwind form

$$u^{n+1}_{j+1/2} = u^n_j, \tag{103}$$

which suggests that $\xi^n_{j+1/2}$ should be chosen as

$$\xi^n_{j+1/2} = \frac{1}{2}\frac{\Delta x}{\Delta t}\frac{1}{c^n_{j+1/2}} = \left(\psi^n_{j+1/2}\right)^{-1}. \tag{104}$$

Remark 6. *An essential property of the kind of flow model we are studying is that the pressure and momentum are inversely related to each other. More precisely, the pressure appears as a flux term in the momentum equations and the momentum appears as a flux term in the pressure equation. This relationship is numerically expressed by the fluxes* (63) *and* (82)*. The inverse relationship between the rescaled viscosities* (104) *is natural in view of this inverse relationship between the pressure and momentum.*

Definition 9. *We will use the term* **RMF-AUSMD** *(Rescaled Mixture Flux AUSMD) to denote the numerical algorithm which is constructed within the discrete frame of* (77)–(80) *where fluxes are given as follows:*

(1) *The numerical flux* $\Lambda^n_{k,j+1/2}$ *is obtained as in* (81)*.*

(2) *We determine* $P^{n+1}_{j+1/2}$ *by considering the following discretization of the pressure evolution equation* (47)

$$\begin{aligned}&\frac{P^{n+1}_{j+1/2} - \frac{1}{2}(p^n_j + p^n_{j+1})}{\Delta t}\\ &= -(\kappa\rho_{\rm l}\xi)^n_{j+1/2}\frac{I^n_{{\rm g},j+1} - I^n_{{\rm g},j}}{\Delta x} - (\kappa\rho_{\rm g}\xi)^n_{j+1/2}\frac{I^n_{{\rm l},j+1} - I^n_{{\rm l},j}}{\Delta x},\end{aligned} \tag{105}$$

where the interface values $\kappa^n_{j+1/2}$ *and* $\rho^n_{k,j+1/2}$ *are computed from* $P^n_{j+1/2}$ *together with the arithmetic average* (81) *which defines* $\alpha^n_{k,j+1/2}$*, and* $\xi^n_{j+1/2}$ *is given by* (104)*.*

(3) *We consider hybrid mass fluxes* $F^n_{k,j+1/2}$ *of the same form as given by* (83) *and* (84)*.*

(a) *For the flux component* $F^{{\rm A},n}_{k,j+1/2}$ *we refer to Section 5.2 and use*

$$F^{{\rm A},n}_{k,j+1/2} = (\rho\alpha v)^{{\rm AUSMD},n}_{k,j+1/2}. \tag{106}$$

(b) *For the flux component* $F^{{\rm D},n}_{k,j+1/2}$ *we use*

$$F^{{\rm D},n}_{k,j+1/2} = \frac{1}{2}(I^n_{k,j} + I^n_{k,j+1}) + \frac{1}{4}\psi^n_{j+1/2}\frac{\Delta x}{\Delta t}(m^n_{k,j} - m^n_{k,j+1}), \tag{107}$$

where $\psi^n_{j+1/2}$ *is given by* (98)*.*

(4) *The flux component* $G^n_{k,j+1/2}$ *is chosen to be consistent with the flux component* $F^{{\rm A},n}_{k,j+1/2}$ *by using*

$$G^n_{k,j+1/2} = G^{{\rm A},n}_{k,j+1/2} = (\rho\alpha v^2)^{{\rm AUSMD},n}_{k,j+1/2}. \tag{108}$$

Definition 10. *We will use the term* **RMF-AUSM$^+$** *to denote the numerical algorithm which is identical to* **RMF-AUSMD** *except from the convective flux terms* $F^{{\rm A},n}_{k,j+1/2}$ *and* $G^{{\rm A},n}_{k,j+1/2}$ *which are defined as follows:*

(a) *For the flux component* $F^{\mathrm{A},n}_{k,j+1/2}$ *we use*

$$F^{\mathrm{A},n}_{k,j+1/2} = (\rho\alpha v)^{\mathrm{AUSM}^+,n}_{k,j+1/2}. \tag{109}$$

(b) *For the flux component* $G^{\mathrm{A},n}_{k,j+1/2}$ *we use*

$$G^{\mathrm{A},n}_{k,j+1/2} = (\rho\alpha v^2)^{\mathrm{AUSM}^+,n}_{k,j+1/2}. \tag{110}$$

To illustrate the basic effect of the RMF strategy, we will also consider a more elementary scheme where the mass fluxes consist of only the F^{D} component.

Definition 11. *We will use the term* **MF-F(D)** *to denote the numerical algorithm which is identical to* **MF-AUSMD** *except from the mass flux terms* $F^{\mathrm{A},n}_{k,j+1/2}$ *which are defined as follows:*

$$F^{\mathrm{A},n}_{k,j+1/2} = F^{\mathrm{D},n}_{k,j+1/2}. \tag{111}$$

Similarly, we will use the term **RMF-F(D)** *to denote the numerical algorithm which is identical to* **RMF-AUSMD** *except from the mass flux terms* $F^{\mathrm{A},n}_{k,j+1/2}$ *which are defined as follows:*

$$F^{\mathrm{A},n}_{k,j+1/2} = F^{\mathrm{D},n}_{k,j+1/2}. \tag{112}$$

7. Numerical Simulations

7.1. **AUSM$^+$ vs PD-AUSM$^+$.** The purpose of this section is to investigate the effect of the pressure diffusion term as described in Section 3.4. We explore the performance for two shock tube problems as well as for the classical water faucet flow problem.

7.1.1. *Toumi's Water-Air Shock.* We consider an initial value problem of a kind introduced by Toumi [25] and investigated by several authors [23, 19, 12]. The initial states are given by

$$\mathbf{W}_{\mathrm{L}} = \begin{bmatrix} p \\ \alpha_{\mathrm{l}} \\ v_{\mathrm{g}} \\ v_{\mathrm{l}} \end{bmatrix} = \begin{bmatrix} 2\cdot 10^7 \text{ Pa} \\ 0.75 \\ 0 \\ 0 \end{bmatrix} \tag{113}$$

and

$$\mathbf{W}_{\mathrm{R}} = \begin{bmatrix} p \\ \alpha_{\mathrm{l}} \\ v_{\mathrm{g}} \\ v_{\mathrm{l}} \end{bmatrix} = \begin{bmatrix} 1\cdot 10^7 \text{ Pa} \\ 0.9 \\ 0 \\ 0 \end{bmatrix}. \tag{114}$$

No source terms are taken into account.

Using the timestep $\Delta x/\Delta t = 1200$ m/s, results for AUSM$^+$ and PD-AUSM$^+$ are given in Figure 1. The computation was performed on a grid of 100 cells for a time of $t = 0.04$ s. For the pressure diffusion term, the value

$$M_0 = 0.2 \tag{115}$$

was used. The MF-AUSMD scheme was used to compute the reference solution, using a fine grid of 10 000 cells.

We observe that severe oscillations are produced using the basic AUSM$^+$. For PD-AUSM$^+$, these oscillations are significantly reduced. However, a slight overshooting behaviour still persists.

The results for PD-AUSM$^+$ are qualitatively consistent with the results reported by Paillère et al [19] for this problem, who considered a full 6-equation model assuming an initial temperature corresponding to athmospheric conditions. The isentropic model with the state equations (12) and (14) we use here assumes an *entropy* corresponding to atmospheric conditions. These approaches give somewhat different results as the conditions of the problem are not atmospheric. In particular we observe a much less dense gas phase as compared to Paillére et al [19].

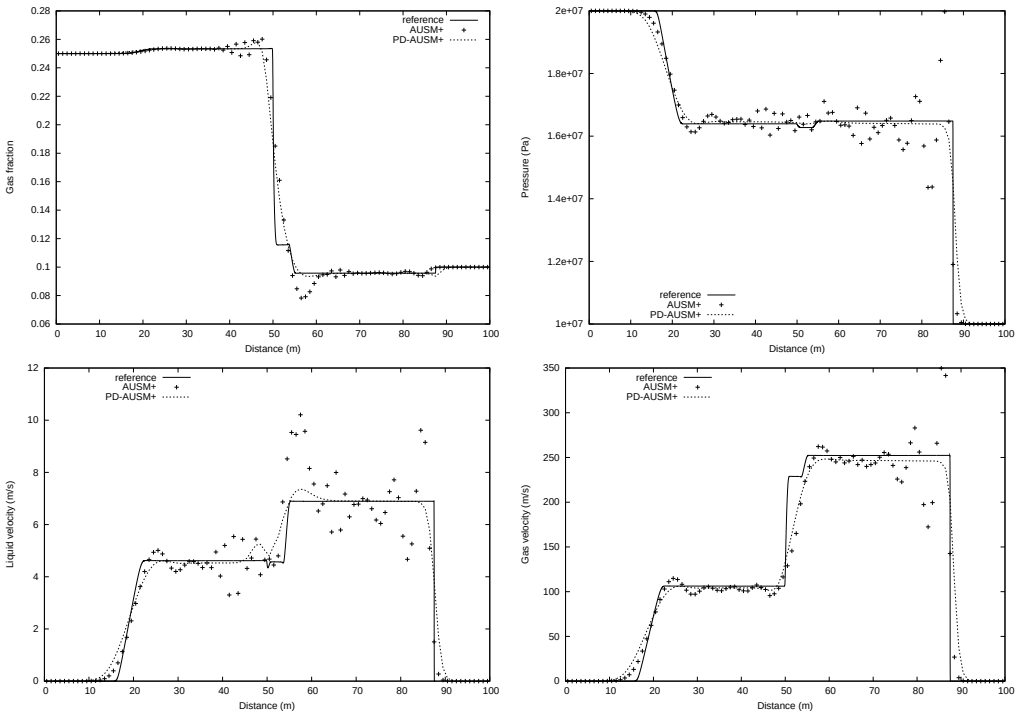

FIGURE 1. Toumi's shock tube problem, 100 cells. AUSM$^+$ vs PD-AUSM$^+$. Top left: Gas fraction. Top right: Pressure. Bottom left: Liquid velocity: Bottom right: Gas velocity.

7.1.2. *A Large Relative Velocity Shock.* We now consider the Riemann problem given by the initial states

$$\mathbf{W}_{\mathrm{L}} = \begin{bmatrix} p \\ \alpha_{\mathrm{l}} \\ v_{\mathrm{g}} \\ v_{\mathrm{l}} \end{bmatrix} = \begin{bmatrix} 265,000 \text{ Pa} \\ 0.71 \\ 65 \text{ m/s} \\ 1 \text{ m/s} \end{bmatrix} \tag{116}$$

and

$$\mathbf{W}_{\mathrm{R}} = \begin{bmatrix} p \\ \alpha_{\mathrm{l}} \\ v_{\mathrm{g}} \\ v_{\mathrm{l}} \end{bmatrix} = \begin{bmatrix} 265,000 \text{ Pa} \\ 0.7 \\ 50 \text{ m/s} \\ 1 \text{ m/s} \end{bmatrix}. \tag{117}$$

Again, no source terms are taken into account. This initial value problem has previously been studied by Cortes et al [5] and Evje and Flatten [10, 11, 12]. In particular, this problem tests the ability of numerical schemes to handle a large velocity difference between the phases.

Using the timestep $\Delta x/\Delta t = 1000$ m/s, results for AUSM$^+$ and PD-AUSM$^+$ are given in Figure 2. The computation was performed on a grid of 100 cells for a time of $t = 0.08$ s. The RMF-AUSMD scheme was used to compute the reference solution, using a fine grid of 10 000 cells. For the pressure diffusion term, the value

$$M_0 = 0.005 \tag{118}$$

was used.

We observe that the basic AUSM$^+$ scheme is stable on the sonic waves. However, severe oscillations are produced around the volume fraction waves. These oscillations are removed for PD-AUSM$^+$, at the price of slightly smearing out the solution.

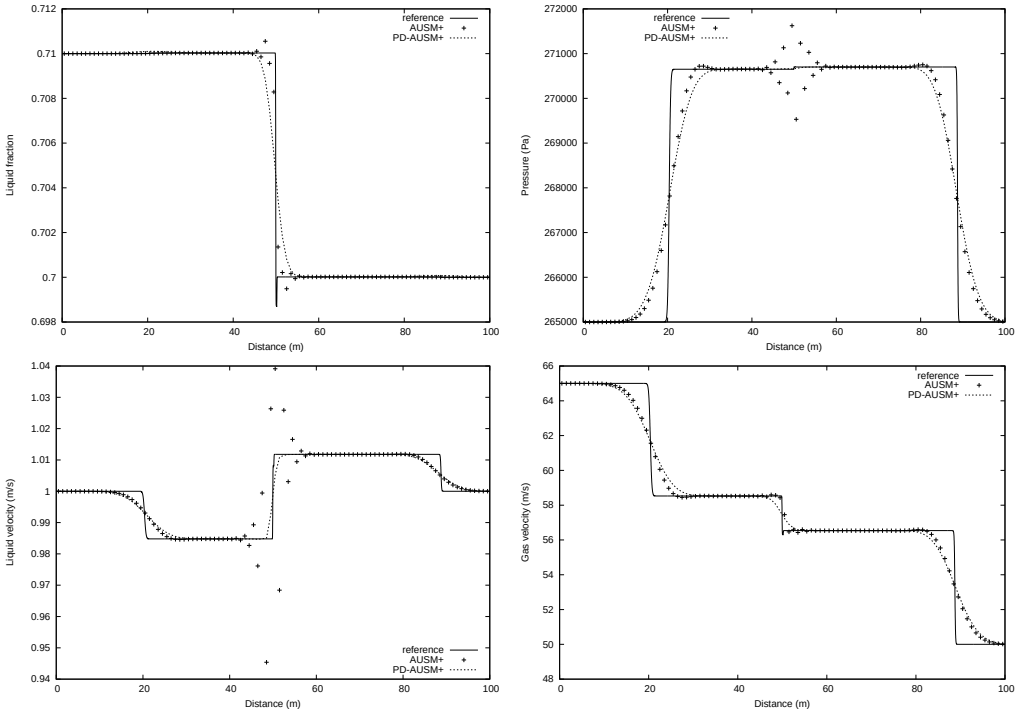

FIGURE 2. LRV shock tube problem, 100 cells. AUSM$^+$ vs PD-AUSM$^+$. Top left: Gas fraction. Top right: Pressure. Bottom left: Liquid velocity: Bottom right: Gas velocity.

7.1.3. *Water faucet.* We now study the classical faucet flow problem of Ransom [20], which has become a standard benchmark [4, 10, 26, 18, 27, 19, 12].

We consider a vertical pipe of length 12 m with the initial uniform state

$$\mathbf{W} = \begin{bmatrix} p \\ \alpha_\mathrm{l} \\ v_\mathrm{g} \\ v_\mathrm{l} \end{bmatrix} = \begin{bmatrix} 10^5 \text{ Pa} \\ 0.8 \\ 0 \\ 10 \text{ m/s} \end{bmatrix}. \tag{119}$$

Gravity is the only source term taken into account, i.e. in the framework of (8) and (9) we have

$$Q_k = g\rho_k\alpha_k, \tag{120}$$

with g being the acceleration of gravity. At the inlet we have the constant conditions $\alpha_\mathrm{l} = 0.8$, $v_\mathrm{l} = 10$ m/s and $v_\mathrm{g} = 0$. At the outlet the pipe is open to the ambient pressure $p = 10^5$ Pa.

We restate the approximate analytical solution presented in the references [10, 27, 19], derived from a simplified model where the pressure variation is neglected.

$$v_\mathrm{l}(x,t) = \begin{cases} \sqrt{v_0^2 + 2gx} & \text{for } x < v_0 t + \frac{1}{2}gt^2 \\ v_0 + gt & \text{otherwise.} \end{cases} \tag{121}$$

$$\alpha_\mathrm{l}(x,t) = \begin{cases} \alpha_0(1 + 2gxv_0^{-2})^{-1/2} & \text{for } x < v_0 t + \frac{1}{2}gt^2 \\ \alpha_0 & \text{otherwise.} \end{cases} \tag{122}$$

Here the parameters $\alpha_0 = 0.8$ and $v_0 = 10$ m/s are the initial states.

In Figure 3 we compare the basic AUSM$^+$ scheme (that is, in the framework of Section 3.4 we consider $M_0 = 1$) and the PD-AUSM$^+$ scheme with $M_0 = 10^{-5}$. A grid of 1200 cells and the timestep $\Delta x/\Delta t = 550$ m/s was used.

We observe that the schemes are inseparable to plotting accuracy, and both schemes produce a slight overshoot in the gas fraction. A similar behaviour was reported by Paillère et al [19], and the

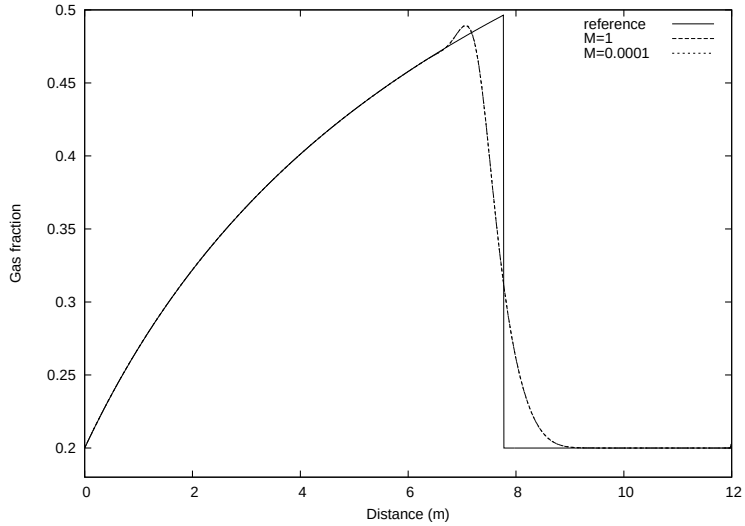

FIGURE 3. Water faucet problem, 1200 cells. AUSM$^+$ ($M_0 = 1$) vs PD-AUSM$^+$ ($M_0 = 10^{-5}$).

basic AUSMD scheme also suffers from this [10]. For this problem the pressure is approximately uniform, hence the pressure diffusion term has little effect.

7.1.4. *Conclusions.* These flow cases illustrate that the basic AUSM$^+$ scheme suffers from a tendency to produce numerical oscillations near discontinuities. The modified PD-AUSM$^+$ is better, altough some oscillatory behaviour still persists. A weakness of the PD-AUSM$^+$ approach is that the diffusion parameter M_0 requires some tuning and may be problem-dependent.

7.2. **Comparison of the MF schemes.** In this section, we compare the performance of MF-AUSMD, MF-AUSM$^+$ and MF-CVS. In particular, it is demonstrated that MF-AUSM$^+$ is a better alternative than PD-AUSM$^+$ for removing numerical oscillations from the basic AUSM$^+$ scheme.

7.2.1. *Toumi's Water-Air Shock.* In Figure 4 the MF-AUSM$^+$, the MF-AUSMD and the MF-CVS schemes are compared. A grid of 100 cells and a timestep $\Delta x/\Delta t = 2000$ m/s was used.

We see that the results represent a significant improvement as compared to the basic AUSM$^+$ scheme of Figure 1. Notably the MF-CVS produces results comparable to the PD-AUSM$^+$ scheme without incorporating free parameters nor a numerical sound velocity.

We observe no oscillatory behaviour around sonic waves. However, a slight difference between the different schemes in the resolution of volume fraction waves is visible. The MF-CVS scheme produces a significant overshoot in the liquid velocity, and we also observe some spurious oscillations for MF-AUSM$^+$. The performance of MF-AUSMD is best.

7.2.2. *Large Relative Velocity Shock.* As can be seen from Figure 2, the volume fraction waves appear as a small wedge near $x = 50$ m. As opposed to the water faucet problem, the volume fraction waves here split into two genuinely non-linear waves moving with different velocities. We now wish to focus more strongly on this phenomenon, and thereby illustrate a basic difference in the dissipative mechanism of MF-CVS and the MF-AUSM schemes.

Focusing the plot around the voulme fraction waves, the MF-AUSM$^+$ and MF-AUSMD schemes are compared in Figure 5, using a grid of size $\Delta x = 0.01$ m. We observe little difference between the schemes.

The MF-CVS scheme is compared with the MF-AUSM$^+$ scheme in Figure 6, using the same computational grid $\Delta x = 0.01$ m. Strong oscillations occur for the MF-CVS scheme.

It is worth noting that the pure advective upwinding (76) used by CVS is the correct upwind form for a *contact discontinuity* of uniform pressure and velocity. Hence we expect MF-CVS to

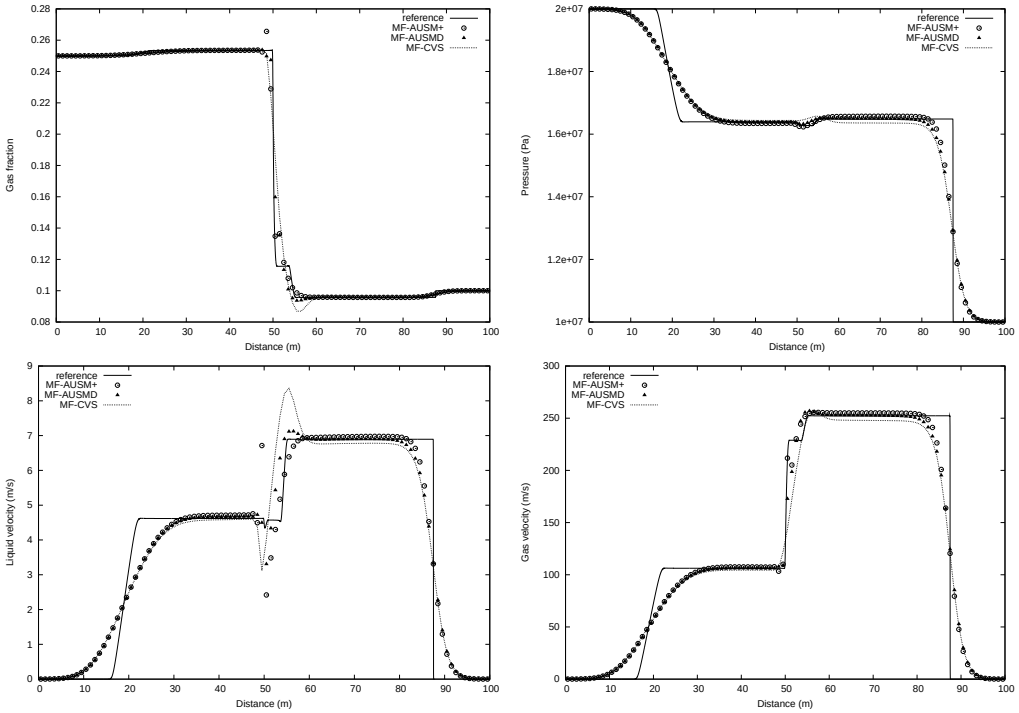

FIGURE 4. Toumi's shock tube problem, 100 cells. MF-AUSM$^+$, MF-AUSMD, MF-CVS. Top left: Gas fraction. Top right: Pressure. Bottom left: Liquid velocity: Bottom right: Gas velocity.

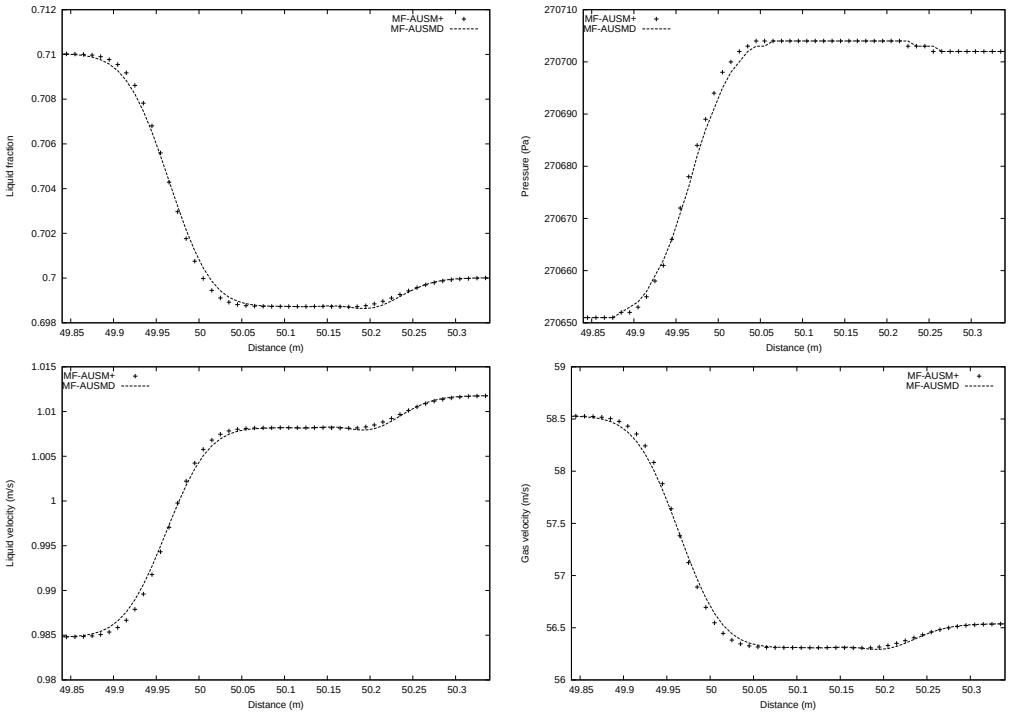

FIGURE 5. LRV shock tube problem, volume fraction waves. 50 cells. MF-AUSM$^+$ vs MF-AUSMD scheme. Top left: Liquid fraction. Top right: Pressure. Bottom left: Liquid velocity: Bottom right: Gas velocity.

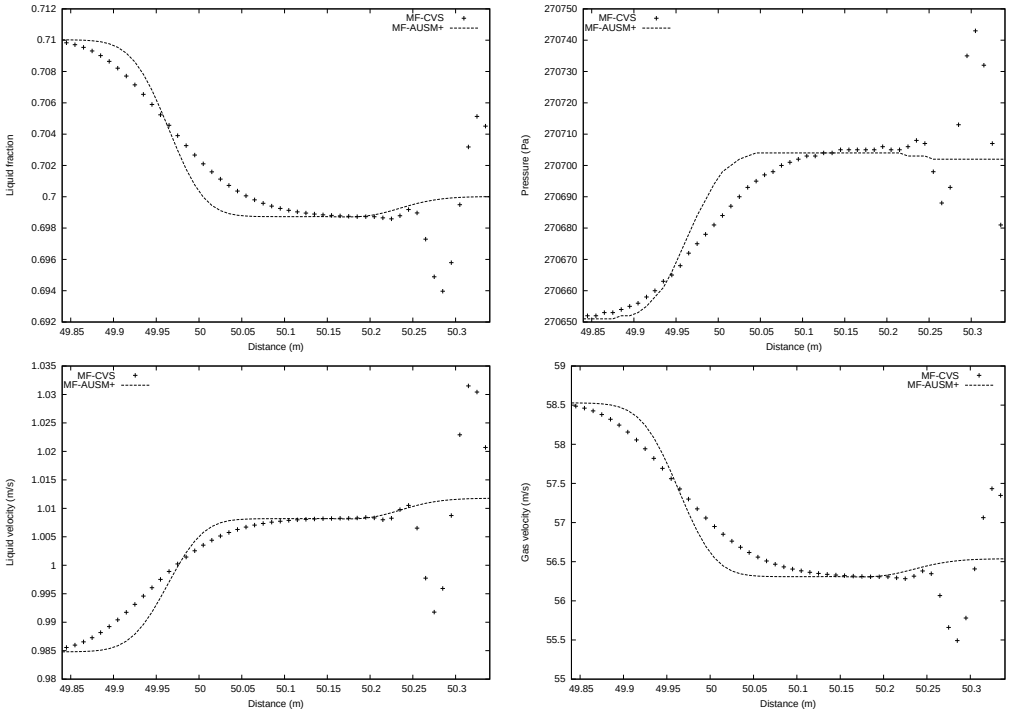

FIGURE 6. LRV shock tube problem, volume fraction waves. 50 cells. MF-AUSM$^+$ vs MF-CVS scheme. Top left: Liquid fraction. Top right: Pressure. Bottom left: Liquid velocity: Bottom right: Gas velocity.

work well for such contact discontinuities (or weakly non-linear waves). However, as this last example shows, the more refined dissipative mechanisms of the MF-AUSM schemes are needed to properly resolve strongly non-linear phenomena in the volume fraction waves.

7.2.3. *Water Faucet.* In Figure 7 we investigate how the different schemes converge to the expected analytical solution for the gas fraction as the grid is refined. There is no significant difference between any of the MF schemes, which all produce non-oscillatory behaviour for this problem. In particular we observe that the overshoot of Figure 3 is removed.

7.2.4. *Conclusions.* MF-AUSM$^+$ represents a better way of introducing the right amount of dissipation for a robust resolution of pressure than PD-AUSM$^+$. No significant differences between MF-AUSM$^+$ and the related MF-AUSMD scheme have been demonstrated. The simpler MF-CVS scheme performs well when the volume fraction waves are essentially linear, as is the case for the water faucet problem, but is inferior to the MF-AUSM schemes in resolving non-linear volume fraction waves.

7.3. **The RMF Strategy.** In this section we apply the rescaling technique descried in Section 6 to the MF-AUSM$^+$ and MF-AUSMD schemes, enabling us to use larger timesteps and achieve a more accurate resolution of sonic waves. In order to demonstrate clearly the impact of the rescaling on the resolution of the sonic waves, we first compare the performance of the MF-F(D) and the RMF-F(D) schemes given by Definition 11. For these schemes the flux component $F_k^A = F_k^D$, hence, we cannot expect an accurate resolution of the volume fraction contact discontinuity. Comparison with a Roe scheme is made. We refer to [10, 26] for a description of the implementation of the Roe scheme.

Next, we compare the RMF-AUSMD and RMF-AUSM$^+$. We shall observe that the rescaling technique reveals a difference in the dissipative mechanisms of AUSM$^+$ and AUSMD regarding their behaviour on sonic waves.

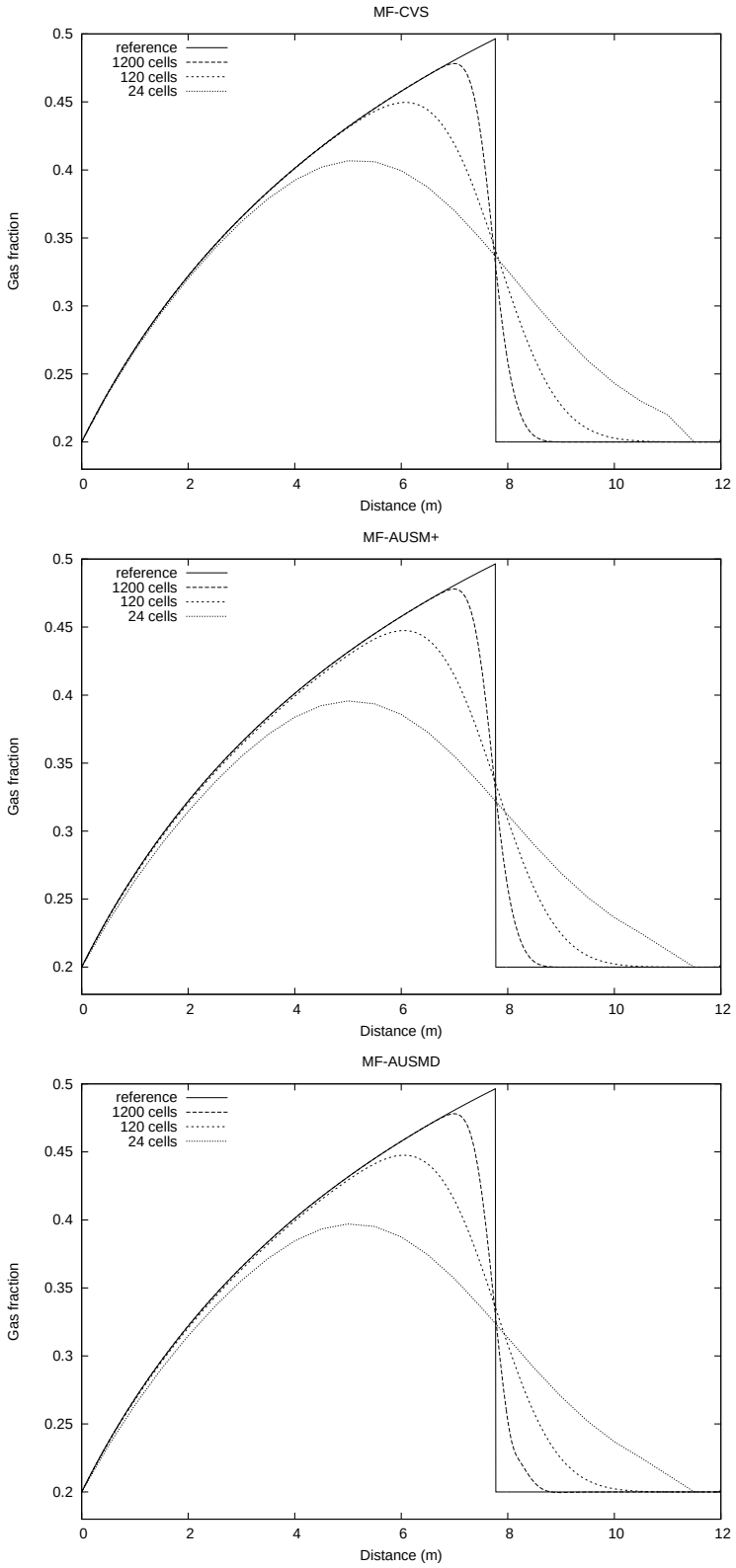

FIGURE 7. Water faucet problem, T=0.6s. Grid refinement for different schemes. Top: MF-CVS scheme. Middle: MF-AUSM$^+$ scheme. Bottom: MF-AUSMD scheme.

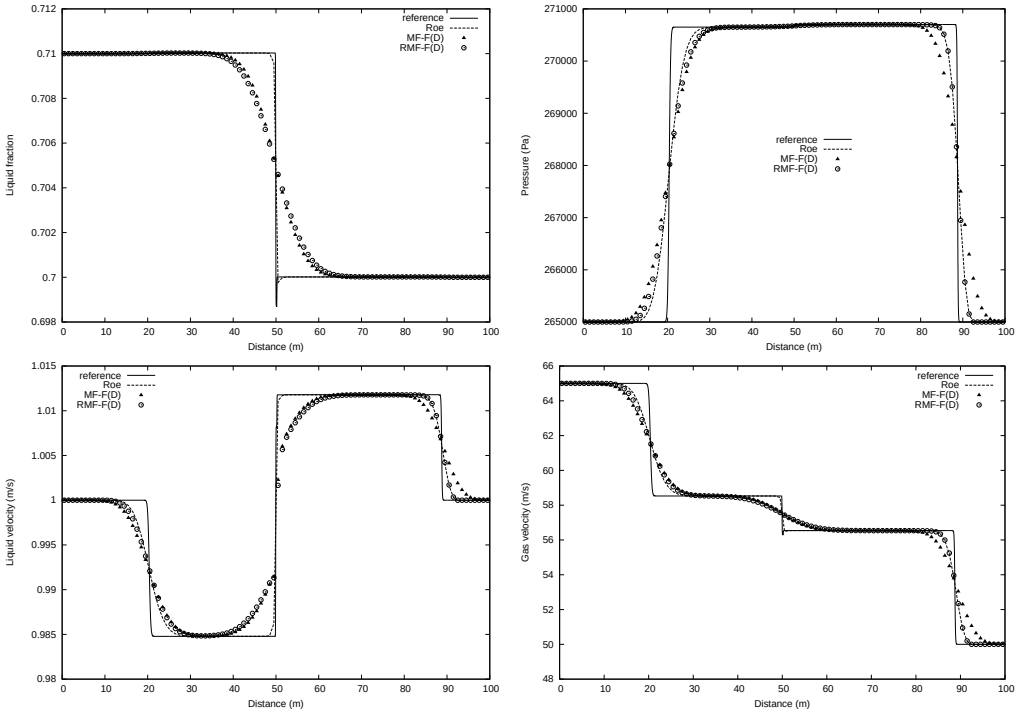

FIGURE 8. LRV shock tube problem, 100 cells. Roe, MF-F(D) and RMF-F(D) scheme. Top left: Liquid fraction. Top right: Pressure. Bottom left: Liquid velocity: Bottom right: Gas velocity.

7.3.1. *Large Relative Velocity Shock.* For the LRV shock, the maximum wave velocity is approximately

$$|\lambda|_{\max} \approx 500\text{m/s}, \tag{123}$$

representing the right-moving sonic wave.

Assuming a grid of 100 cells, numerical investigations reveal the critical timestep to be

$$\Delta x/\Delta t = 525 \text{ m/s} \tag{124}$$

for the RMF schemes, and more strictly

$$\Delta x/\Delta t = 660 \text{ m/s} \tag{125}$$

for the basic MF schemes. Hence the RMF schemes allow for larger timesteps and more efficient integration.

In Figure 8 we compare the Roe scheme, the MF-F(D) scheme and the RMF-F(D) scheme using a grid of 100 cells. Here the timestep (124) is used for the Roe and RMF-F(D) scheme, whereas (125) is used for the MF-F(D) scheme. We observe that RMF-F(D) produces a non-oscillatory approximation of the sonic waves, while noticably improving the approximation properties of the basic F(D) flux. We obtain an accuracy on sonic waves comparable with the Roe scheme, and the RMF strategy works as intended.

In Figure 9, RMF-AUSMD and RMF-AUSM$^+$ are compared to the RMF-F(D) scheme using a grid of 100 cells and the timestep (124). The RMF-AUSMD is able to preserve the basic stability properties of RMF-F(D), while being significantly more accurate on the volume fraction waves. However, RMF-AUSM$^+$ introduces small overshoots as compared to RMF-F(D). This comparison reveals that the AUSMD fluxes seems to be more consistent with the MF approach than the AUSM$^+$ fluxes.

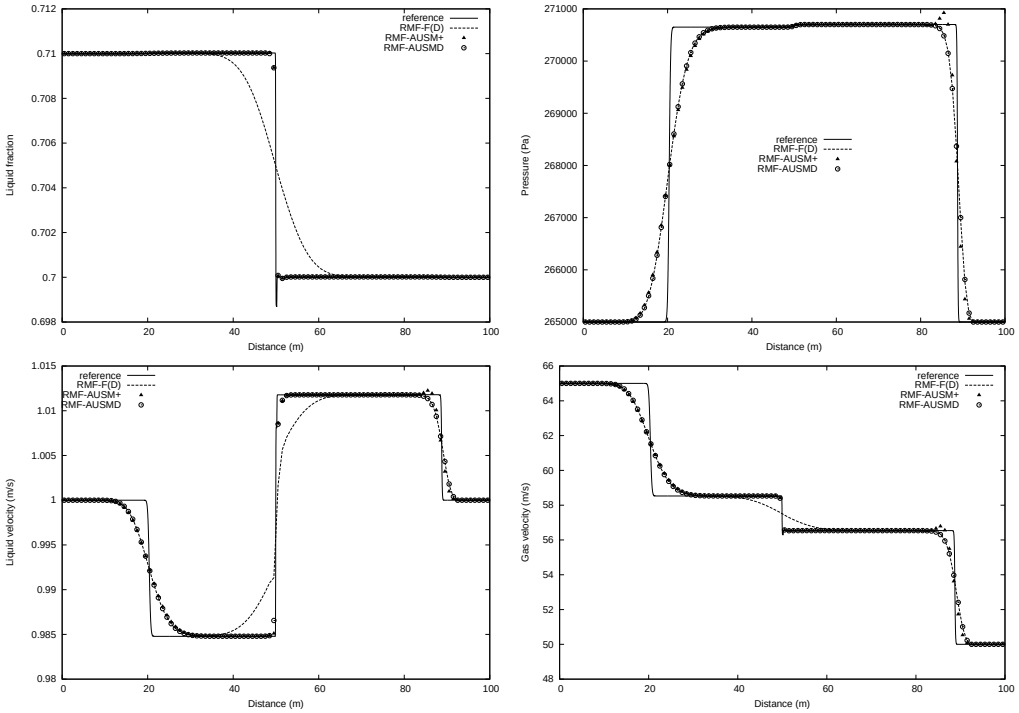

FIGURE 9. LRV shock tube problem, 100 cells. RMF-F(D), RMF-AUSM$^+$ and RMF-AUSMD scheme. Top left: Liquid fraction. Top right: Pressure. Bottom left: Liquid velocity: Bottom right: Gas velocity.

7.3.2. *Toumi's Water-Air Shock.* Results are given in Figure 10 for the RMF-AUSM$^+$ scheme and RMF-AUSMD scheme, using a grid of 100 cells and a timestep

$$\frac{\Delta x}{\Delta t} = 1140 \text{ m/s}. \tag{126}$$

We observe that the sonic waves are reproduced with less numerical diffusion as compared to Figure 4. There is an overshoot in the right-going (fastest) sonic wave for RMF-AUSM$^+$, whereas RMF-AUSMD has no such problems.

7.3.3. *Water Faucet.* As observed for the shock tube problems, we found that the viscosity rescaling allows us to use a bigger timestep for the numerical integration. In particular, we found the critical timestep to be $\Delta x/\Delta t = 540$ m/s for the basic MF schemes and

$$\frac{\Delta x}{\Delta t} = 390 \text{ m/s} \tag{127}$$

for the RMF schemes.

In Figure 11 the RMF-AUSM$^+$ scheme is compared to the RMF-AUSMD scheme for $T = 0.6$ s on a grid of 120 computational cells, using the timestep $\Delta x/\Delta t = 390$ m/s. The schemes are inseparable to plotting accuracy.

7.3.4. *Conclusions.* The viscosity rescaled RMF-AUSM$^+$ and RMF-AUSMD allow for higher integration timesteps than the basic MF-AUSM$^+$ and MF-AUSMD schemes. A difference between the inherent robustness properties of AUSM$^+$ and AUSMD manifests itself on the resolution of sonic waves. More precisely, we observe that the RMF-AUSMD scheme is robust whereas the RMF-AUSM$^+$ scheme may induce oscillations around sonic shocks.

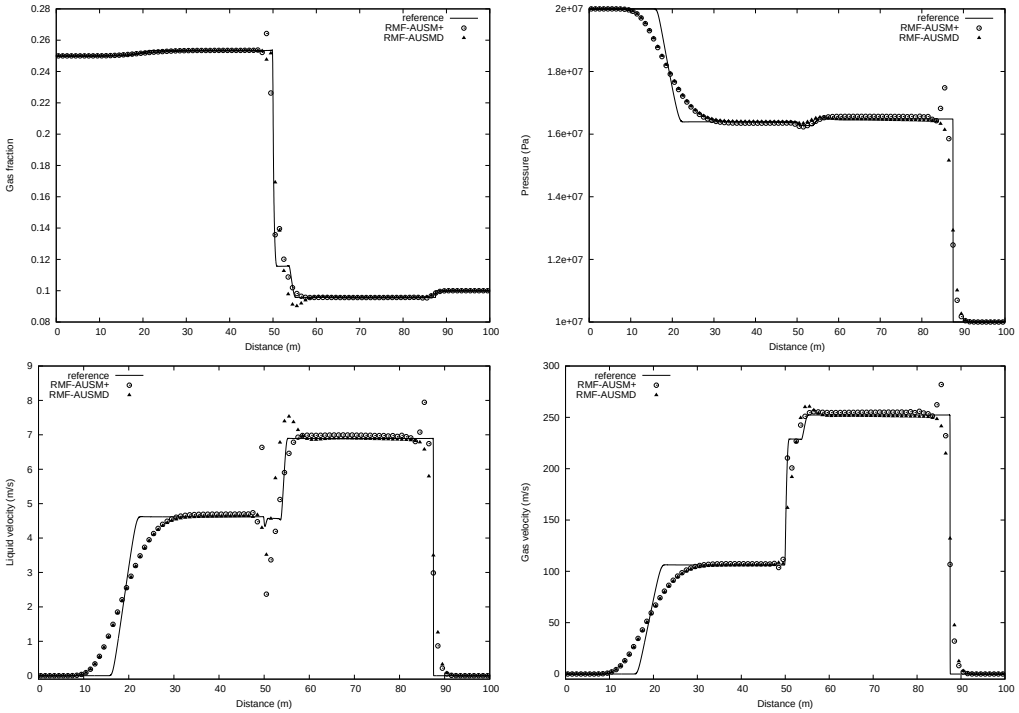

FIGURE 10. Toumi's shock tube problem, 100 cells. RMF-AUSM$^+$ vs RMF-AUSMD. Top left: Gas fraction. Top right: Pressure. Bottom left: Liquid velocity: Bottom right: Gas velocity.

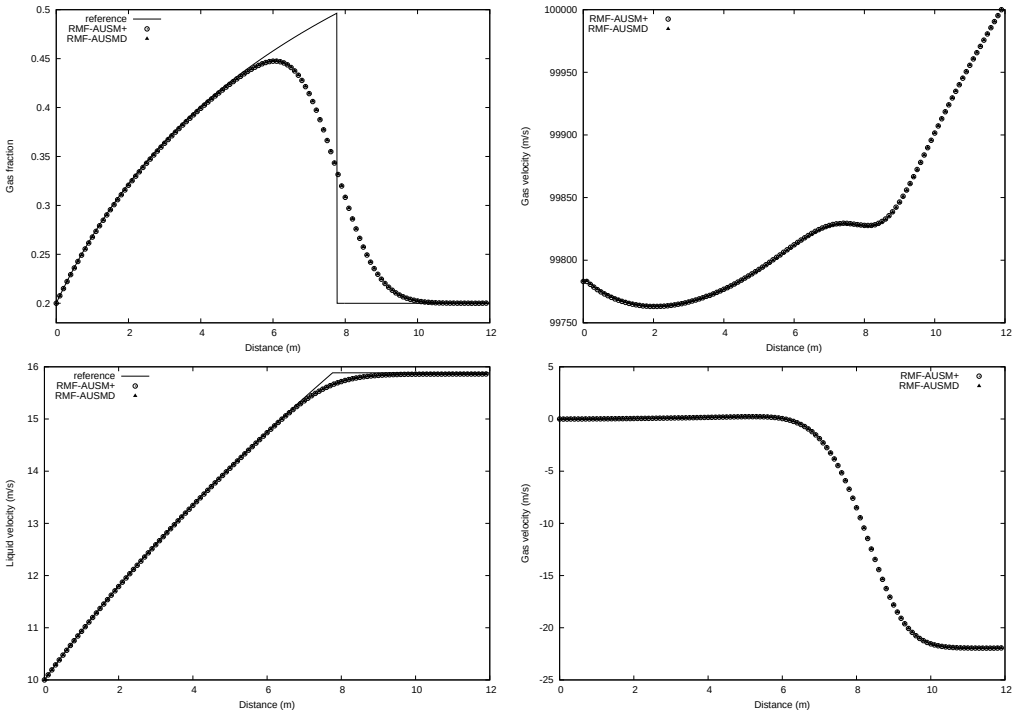

FIGURE 11. Water faucet problem, 120 cells. RMF-AUSM$^+$ vs RMF-AUSMD scheme. Top left: Gas fraction. Top right: Pressure. Bottom left: Liquid velocity: Bottom right: Gas velocity.

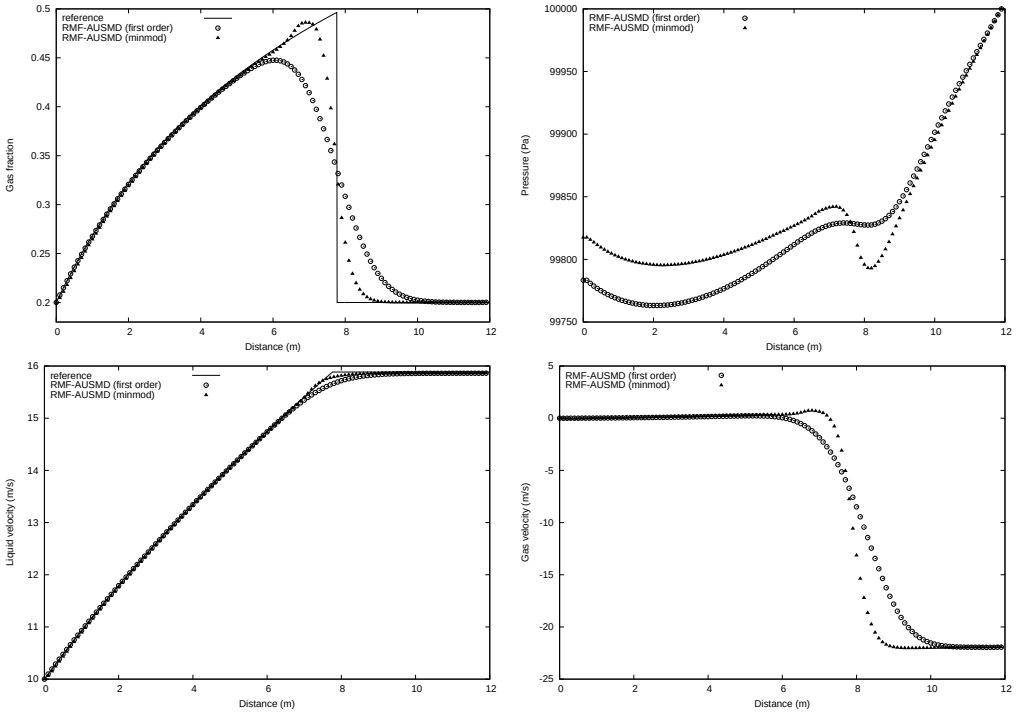

FIGURE 12. Water faucet problem, 120 cells. First order vs minmod RMF-AUSMD. Top left: Gas fraction. Top right: Pressure. Bottom left: Liquid velocity: Bottom right: Gas velocity.

7.4. **Extensions to Higher Order Spatial Accuracy.** In this section, we illustrate the possibility of achieving higher order spatial accuracy by adapting the MUSCL strategy of van Leer [14]. Following [15, 8], we apply a slope-limiting procedure to the *primitive* variables

$$\mathbf{W} = \begin{bmatrix} p \\ \alpha_{\mathrm{l}} \\ v_{\mathrm{g}} \\ v_{\mathrm{l}} \end{bmatrix} \tag{128}$$

to calculate new interface values $\hat{\mathbf{U}}_j^{\mathrm{L}}(\mathbf{W}_{j-1}, \mathbf{W}_j, \mathbf{W}_{j+1})$ and $\hat{\mathbf{U}}_j^{\mathrm{R}}(\mathbf{W}_{j-1}, \mathbf{W}_j, \mathbf{W}_{j+1})$. We now modify the convective fluxes F_k^{A} and G_k^{A} of Definition 5 as follows:

$$\hat{F}_{j+1/2}^{\mathrm{A}} = F^{\mathrm{A}}(\hat{\mathbf{U}}_j^{\mathrm{R}}, \hat{\mathbf{U}}_{j+1}^{\mathrm{L}}) \tag{129}$$

and

$$\hat{G}_{j+1/2}^{\mathrm{A}} = G^{\mathrm{A}}(\hat{\mathbf{U}}_j^{\mathrm{R}}, \hat{\mathbf{U}}_{j+1}^{\mathrm{L}}). \tag{130}$$

where we use the "minmod" slope-limiter.

Remark 7. *In general, one could explore applying a slope-limiting procedure also on the pressure evolution equation* (47) *and the flux component* F_k^{D}*, aiming for higher order accuracy on the pressure waves. In this paper, we restrict ourselves to demonstrating that the above simple procedure allows for improved accuracy on the volume fraction waves without sacrificing stability on the pressure waves.*

7.4.1. *Water Faucet.* In Figure 12 the first order and minmod RMF-AUSMD schemes are compared, using a grid of 120 computational cells.

We observe that the minmod strategy allows for significantly improved accuracy, at the price of introducing slight overshoots. These overshoots seem to decay with grid refinement, as is illustrated in Figure 13.

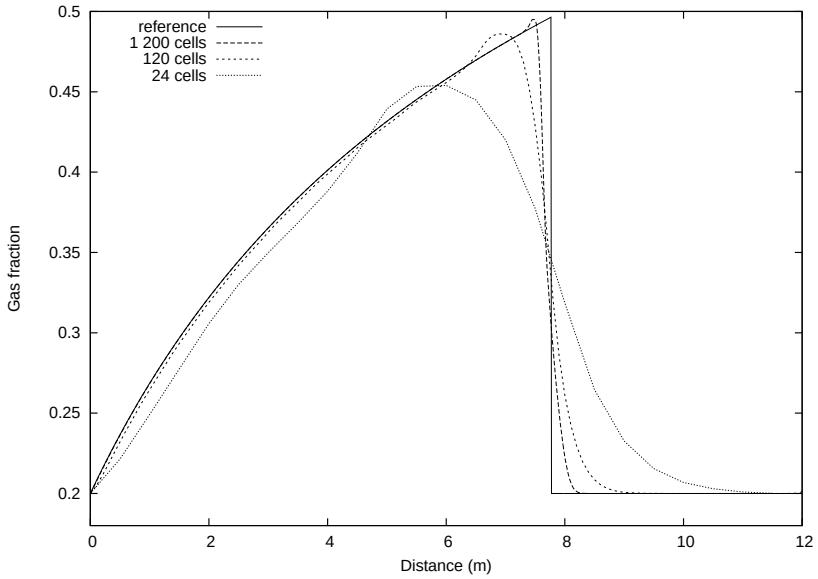

FIGURE 13. Water faucet problem. Grid convergence for the minmod RMF-AUSMD scheme.

7.4.2. *Separation Problem.* We now consider the separation problem introduced by Coquel et al [4], previously investigated by Paillère et al [19] and Evje and Flatten [10, 11, 12]. The problem consists of a vertical pipe of length 7.5 m, initially filled with stagnant liquid and gas with a uniform pressure of $p_0 = 10^5$ Pa, and a uniform liquid fraction of $\alpha_{\rm l} = 0.5$. The pipe is considered to be closed at both ends, i.e. both phasic velocities are forced to be zero at the end points.

Assuming that the phases are accelerated by gravity only, the following approximate analytical solution was presented in [10]

$$\alpha_{\rm l}(x,t) = \begin{cases} 0 & \text{for } x < \frac{1}{2}gt^2 \\ 0.5 & \text{for } \frac{1}{2}gt^2 \le x < L - \frac{1}{2}gt^2 \\ 1 & \text{for } L - \frac{1}{2}gt^2 < x \end{cases} \tag{131}$$

where $L = 7.5$ m is the length of the tube. This approximate solution consists of a "contact" wave at the top of the tube and a shock wave forming at the bottom. After the time

$$T = \sqrt{\frac{L}{g}} = 0.87 \text{ s}, \tag{132}$$

these discontinuities will merge and the phases become fully separated. The volume fraction reaches a stationary state, whereas the other variables slowly converge towards a stationary solution. In particular we expect the stationary pressure to be fully hydrostatic, approximately given by

$$p(x,t) = \begin{cases} p_0 & \text{for } x < L/2 \\ p_0 + \rho_{\rm l} g\,(x - L/2) & \text{for } x \ge L/2. \end{cases} \tag{133}$$

7.4.3. *Transition to One-Phase Flow.* It has previously been observed that the basic MF-AUSMD scheme may produce instabilities as the limit $\alpha_{\rm g,l} = 0$ is approached [12]. The minmod RMF-AUSMD scheme has a similar behaviour, and a modification is required for a stable numerical transition to one-phase flow.

We will here follow an approach similar to the one used in [12]. The approach may be described by two steps:

(1) *Removal of numerical stiffness.* The idea is to replace the RMF-AUSMD scheme with a more dissipative scheme near one-phase regions, as described by the following definition

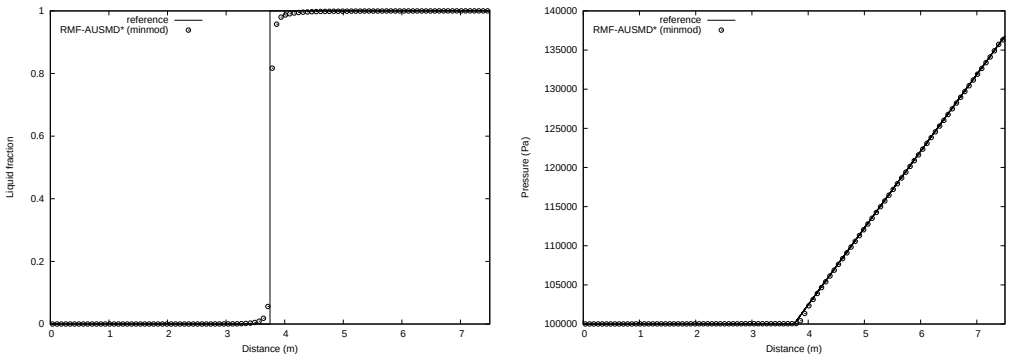

FIGURE 14. Separation problem, T=1.5 s. RMF-AUSMD* with minmod limiter, 100 cells. Top left: Liquid fraction. Top right: Pressure. Bottom left: Liquid velocity. Bottom right: Gas velocity.

Definition 12. *We consider a hybrid of the RMF-AUSMD and the van Leer scheme, denoted as* **RMF-AUSMD***, *where the numerical mass fluxes are given by the following expression*

$$\mathbf{F}^{\mathrm{RMF-AUSMD}^*} = s\mathbf{F}^{\text{van Leer}} + (1-s)\mathbf{F}^{\mathrm{RMF-AUSMD}}. \tag{134}$$

Here s is chosen as

$$s = \max(\phi_{\mathrm{L}}, \phi_{\mathrm{R}}), \tag{135}$$

where ϕ is an indicator function designed to be 1 near one-phase regions, 0 otherwise. The momentum fluxes are unchanged.

For the purposes of this paper we choose

$$\phi_j = e^{-k[\alpha_{\mathrm{g}}]_j^n} + e^{-k[\alpha_{\mathrm{l}}]_j^n} \tag{136}$$

where we use the parameter $k = 50$. In addition, the minmod limiter is used both on the RMF-AUSMD component and the van Leer component.

(2) *Removal of unphysical velocity gradients.* With no friction forces acting upon the phases, the hydrostatic pressure gradients will induce an acceleration of the light gas phase as $\alpha_{\mathrm{g}} \to 0$. The resulting large velocity gradients are unphysical, as in reality we expect the last remnants of gas to be dissolved in the liquid, yielding $v_{\mathrm{g}} \approx v_{\mathrm{l}}$.

To remedy this, we follow the approach of Paillére et al [19], and include an interface momentum exchange term on the form

$$M_{\mathrm{g}}^{\mathrm{D}} = C\alpha_{\mathrm{g}}\alpha_{\mathrm{l}}\rho_{\mathrm{g}}(v_{\mathrm{g}} - v_{\mathrm{l}}), \tag{137}$$

where $C > 0$ and $M_{\mathrm{l}}^{\mathrm{D}} = -M_{\mathrm{g}}^{\mathrm{D}}$, conserving total momentum. For the coefficient C we choose

$$C = C_0 e^{-k[\alpha_{\mathrm{g}}]_j^n}, \tag{138}$$

where $C_0 = 3000\ \mathrm{s}^{-1}$.

Results after $T = 1.5$ s are plotted in Figure 14, using a grid of 100 cells and a timestep $\Delta x/\Delta t = 650$ m/s. At this point stationary conditions are reached. The phases are separated, and the expected hydrostatic pressure gradient is recovered.

A comparison between the minmod and first order RMF-AUSMD* schemes during the transient period is given in Figure 15, where we consider the effect of grid refinement. As expected, we observe a significant improvement in accuracy for the minmod scheme.

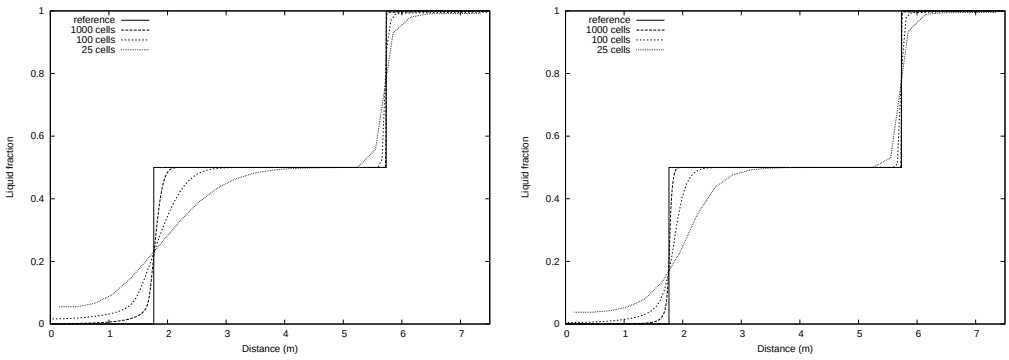

FIGURE 15. Separation problem, T=0.6 s. Grid refinement for the RMF-AUSMD* scheme. Left: First order. Right: Minmod.

8. SUMMARY

In this paper, we have investigated several aspects of AUSM type schemes for a two-phase flow model. Our conclusions may be summarized as follows:

- The basic AUSM$^+$ scheme is highly oscillatory around discontinuities. In particular, AUSM$^+$ lacks robustness around sonic waves. Additional dissipative terms are required to stabilize AUSM$^+$.
- Paillére et al [19] investigated the effect of a *pressure diffusion term*, resulting in the scheme denoted as PD-AUSM$^+$ in this paper. We have demonstrated that the *mixture flux* (MF) strategy of Flåtten and Evje [12] may be applied to AUSM$^+$, and the resulting MF-AUSM$^+$ is more robust than PD-AUSM$^+$.
- There is little difference between the MF-AUSMD and the MF-AUSM$^+$ schemes. However, they are both superior to a simple one-sided advective splitting, the MF-CVS, in robustness on volume fraction waves.
- We have introduced a viscosity rescaling technique allowing us to relax the timestep restriction for the MF schemes. Within this framework, denoted as *Rescaled Mixture Flux* (RMF), the poorer stability properties of AUSM$^+$ on sonic waves resurface. We observe that the RMF-AUSMD is superior to RMF-AUSM$^+$ in robustness on sonic waves.
- The MUSCL strategy has been successfully applied to the RMF-AUSMD scheme, allowing for higher order accuracy on the volume fraction waves.

In particular, we have generalised the mixture flux strategy introduced in [12]. Within the MF framework, the AUSMD seems the most promising candidate for the convective flux splittings.

Acknowledgements. The first author thanks the Norwegian Research Council for financial support through the "Petronics" programme.

REFERENCES

[1] R. Abgrall, How to prevent pressure oscillations in multicomponent flow calculations, *J. Comput. Phys.* **125**, 150–160, 1996.
[2] F. Barre et al. The cathare code strategy and assessment, *Nucl. Eng. Des.* **124**, 257–284, 1990.
[3] K. H. Bendiksen, D. Malnes, R. Moe, and S. Nuland, The dynamic two-fluid model OLGA: Theory and application, in *SPE Prod. Eng.* **6**, 171–180, 1991.
[4] F.Coquel, K. El Amine, E. Godlewski, B. Perthame, and P. Rascle, A numerical method using upwind schemes for the resolution of two-phase flows, *J. Comput. Phys.* **136**, 272–288, 1997.
[5] J. Cortes, A. Debussche, and I. Toumi, A density perturbation method to study the eigenstructure of two-phase flow equation systems, *J. Comput. Phys.* **147**, 463–484, 1998.
[6] J. R. Edwards, R. K. Franklin, and M.-S. Liou, Low-diffusion flux-splitting methods for real fluid flows with phase transition, *AIAA Journal* **38**, 1624-1633, 2000.
[7] J. R. Edwards and M.-S. Liou, Low-diffusion flux-splitting methods for flows at all speeds, *AIAA Journal* **36**, 1610-1617, 1998.

[8] S. Evje and K. K. Fjelde, Hybrid flux-splitting schemes for a two-phase flow model, *J. Comput. Phys.* **175**, 674–701, 2002.
[9] S. Evje and K. K. Fjelde, On a rough ausm scheme for a one-dimensional two-phase flow model, *Comput. & Fluids* **32**, 1497–1530, 2003.
[10] S. Evje and T. Flåtten. Hybrid flux-splitting schemes for a common two-fluid model. *J. Comput. Phys*, in press.
[11] S. Evje and T. Flåtten. Weakly implicit numerical schemes for the two-fluid model. Submitted for publication, August 2003.
[12] T. Flåtten and S. Evje. A mixture flux approach for accurate and robust resolution of two-phase flows. Submitted for publication, July 2003.
[13] M. Larsen, E. Hustvedt, P. Hedne, and T. Straume, Petra: A novel computer code for simulation of slug flow, in *SPE Annual Technical Conference and Exhibition*, SPE 38841, p. 1–12, October 1997.
[14] B. V. Leer, Towards the ultimate conservative difference scheme V. A second-order sequel to Godunov's method, *J. Comput. Phys.* **32**, 101–136, 1979.
[15] M.-S. Liou, A sequel to AUSM: AUSM(+), *J. Comput. Phys.* **129**, 364–382, 1996.
[16] M.-S. Liou and C. J. Steffen, A new flux splitting scheme, *J. Comput. Phys.* **107**, 23-39, 1993.
[17] Y. Y. Niu, Simple conservative flux splitting for multi-component flow calculations, *Num. Heat Trans.* **38**, 203-222, 2000.
[18] Y.-Y. Niu, Advection upwinding splitting method to solve a compressible two-fluid model, *Int. J. Numer. Meth. Fluids* **36**, 351–371, 2001.
[19] H. Paillère, C. Corre and J.R.G Cascales, On the extension of the AUSM+ scheme to compressible two-fluid models, *Comput. & Fluids* **32**, 891–916, 2003.
[20] V. H. Ransom, Numerical bencmark tests, *Multiphase Sci. Tech.* **3**, 465-473, 1987.
[21] R. Saurel and R. Abgrall, A multiphase Godunov method for compressible multifluid and multiphase flows, *J. Comput. Phys.* **150**, 425–467, 1999.
[22] R. Saurel and R. Abgrall, A simple method for compressible multifluid flows, *SIAM J. Sci. Comp.* **21**, 1115–1145, 1999.
[23] I. Tiselj and S. Petelin, Modelling of two-phase flow with second-order accurate scheme, *J. Comput. Phys.* **136**, 503–521, 1997.
[24] E. Tadmor. Numerical viscosity and the entropy condition for conservative difference schemes. *Mathematics of Computation.* **43**, 369–381, 1984.
[25] I. Toumi, An upwind numerical method for two-fluid two-phase flow models, *Nuc. Sci. Eng.* **123**, 147–168, 1996.
[26] I. Toumi and A. Kumbaro, An approximate linearized riemann solver for a two-fluid model, *J. Comput. Phys.* **124**, 286–300, 1996.
[27] J. A. Trapp and R. A. Riemke, A nearly-implicit hydrodynamic numerical scheme for two-phase flows, *J. Comput. Phys.* **66**, 62–82, 1986.
[28] Y. Wada and M.-S. Liou, An accurate and robust flux splitting scheme for shock and contact discontinuities, *SIAM J. Sci. Comput.* **18**, 633–657, 1997.